Combust. Sci. and Tech., 1993, Vol. 90, pp. 1-34
Photocopying permitted by license only

©Gordon and Breach Science Publishers S.A.
Printed in United States of America

Comparison of Experimental and Computed Species Concentration and Temperature Profiles in Laminar, Two-Dimensional Methane/Air Diffusion Flames

THOMAS S. NORTON[1] and KERMIT C. SMYTH *Building and Fire Research Laboratory, National Institute of Standards and Technology, Gaithersburg, MD 20899*

J. HOUSTON MILLER *Department of Chemistry, The George Washington University, Washington, DC 20052*

and MITCHELL D. SMOOKE *Department of Mechanical Engineering, Yale University, New Haven, CT 06520*

(Received March 18, 1992; in final form June 23, 1992)

Abstract—Experimental concentration measurements of the major stable species and five radical species (OH·, H atom, O atom, CH·, and CH_3·) obtained on a rectangular Wolfhard-Parker slot burner are compared with a detailed computation of the chemical structure of an axisymmetric laminar, CH_4/air diffusion flame burning at atmospheric pressure. In order to examine these CH_4/air flames with different geometries and different sizes, the species profiles are plotted as functions of the local mixture fraction, and the scalar dissipation rate has been matched in a region around the stoichiometric surface. The overall agreement in the absolute concentrations, the shape of the profiles, and their location in terms of the local mixture fraction is good to excellent for the stable species (except for O_2) and for the most abundant radicals OH·, H atom, and O atom. For example, the calculated OH· maximum concentration is in much better agreement with the experimental results than are full equilibrium and partial equilibrium estimates. Less satisfactory agreement is found for the CH· and CH_3· radicals. In addition, significant discrepancies are observed in the temperature field and in the degree of O_2 penetration into rich flame regions.

NOMENCLATURE

[A]	concentration of species A
c_p	average specific heat at constant pressure for the local gas mixture
D	diffusion coefficient
H	height above the burner (rectangular slot burner)
k	arbitrary constant
Le	Lewis number
m_i	mass flow rate of species i
P	pressure
r	radial position coordinate (axisymmetric burner)
T	temperature
t	time
v	velocity
x	lateral position coordinate (rectangular slot burner)
y	longitudinal position coordinate (rectangular slot burner)
z	height above the burner (axisymmetric burner)
W_{avg}	average molecular weight
W_i	molecular weight of species or element i
X_i	mole fraction of species i

[1] NRC-NIST Postdoctoral Research Associate (1990-1991); current address: Morgantown Energy Technology Center, Morgantown, West Virginia 26505.

Y_i mass fraction of species i
Z_i mass fraction of element i (e.g. Z_C, Z_O)
β arbitrary linear combination of conserved scalars
λ thermal conductivity
ξ mixture fraction
ρ density
ϕ equivalence ratio
χ scalar dissipation rate
ω_i net chemical production rate for species i

Subscripts:
1 limiting value in the fuel stream (e.g. β_1, $Z_{C,1}$)
2 limiting value in the oxidizer stream (e.g. β_2, $Z_{O,2}$)
B as defined by R.W. Bilger (e.g. ξ_B)
i individual species or element (e.g. ξ_H, ξ_C, W_O)
s stoichiometric surface (e.g. x_s, ξ_s, χ_s)

I INTRODUCTION

The last decade has witnessed significant advances in our knowledge of both the chemical reactions which occur under high-temperature combustion conditions and the associated fluid mechanical mixing processes. As a consequence, increasing attention is now focused on improving our understanding of the typically strong coupling between chemical heat release and turbulent mixing, i.e. chemistry-turbulence interactions. One approach for including chemical reactions in computational models of turbulent diffusion flames is to utilize libraries of strained laminar flame calculations (Liew *et al.*, 1981, 1984; Peters, 1984, 1986) which incorporate detailed reaction mechanisms (Rogg *et al.*, 1986; Haworth *et al.*, 1988). An alternative avenue is to reduce systematically the number of chemical steps in the basic oxidation mechanisms for combustion to as few as possible (typically three or four), while still providing an adequate description of the major species concentration and temperature profiles (Paczko *et al.*, 1986; Peters and Kee, 1987; Bilger *et al.*, 1990; Wang and Frenklach, 1991).

Few studies have addressed the question of how well flame structure calculations reproduce experimental results. Recent work, mostly in turbulent jet diffusion flames of diluted methane, has compared measured concentrations of the OH· radical and the major stable species to values computed for strained (counterflow) laminar flames (Barlow *et al.* 1990a, 1990b; Barlow and Collignon, 1991). With respect to developing reduced chemical mechanisms, most of the effort has used a detailed flame structure calculation as the point of reference (for example, see Smooke, 1991). Although both strategies are logical, to this point only limited comparisons have been made between experimental measurements and detailed flame structure computations for laminar diffusion flames, particularly for the radical species (Barlow and Collignon, 1991).

In the last several years we have undertaken a detailed experimental investigation of a laminar, CH_4/air diffusion flame, in which measurements have been made of species concentrations, velocity, and temperature (Smyth *et al.*, 1985). In addition to mass spectrometric detection of stable molecules, radical concentration profiles have been obtained for CH_3· (Smyth and Taylor, 1985; Miller and Taylor, 1987), OH· (Smyth *et al.*, 1990), H atom (Smyth and Tjossem, 1990a), O atom (Smyth and Tjossem, 1990a), and CH· (Norton and Smyth, 1991). Beyond these results, profile data for radicals in laminar hydrocarbon diffusion flames are scarce. Melvin and Moss (1975) have reported an OH· profile in a N_2-diluted CH_4/air flame, Bastin *et al.* (1987) have used molecular

beam mass spectrometry to sample numerous radicals in a 30-torr $C_2H_2/O_2/Ar$ flame, and Barlow and Collignon (1991) have obtained OH· profiles in both counterflow and co-flow air-diluted methane flames.

The detailed experimental profile measurements which are now available in the undiluted CH_4/air diffusion flame enable a much more complete comparison to be made with flame structure calculations than has been possible before. Our initial focus has been on the radical species H·, O:, OH·, CH·, and CH_3· (Miller and Smyth, 1990), since minor species concentrations generally provide more critical and demanding tests of mechanism and model predictions than do the major species (Westmoreland *et al.*, 1986). However, in our analysis it has become evident that the major stable species also need attention.

Some initial comparisons between experimental measurements and flame structure calculations have been carried out for two-dimensional axisymmetric CH_4/air diffusion flames (Smooke *et al.*, 1989, 1990). The agreement is generally good for the major stable species and provides confidence in the chemical mechanism used in the flame structure calculations (Puri *et al.*, 1987). The present paper extends the comparisons between experimental data and flame structure predictions in two-dimensional CH_4/air diffusion flames, with particular emphasis on the radical species. Since our experimental measurements have been made on a rectangular Wolfhard-Parker burner, in contrast to the axisymmetric geometry of the flame structure computation (see Section III), it is also necessary to examine the results using geometry-independent coordinates, such as the local mixture fraction and the scalar dissipation rate. These parameters are of interest for describing the chemical composition and the strain field in laminar flamelet approaches. In order to address the question of which library of laminar flamelets is the best to use for turbulent flame computations, comparisons will also need to be made between counterflow and co-flow geometries. The present study is a first step in assessing how well comparisons can be made for diffusion flames in geometry-independent coordinates. On balance our findings indicate that the flame structure calculations for the relatively simple case of a CH_4/air diffusion flame agree as well with experimental results as predictions in premixed flames, such as the study of Westmoreland *et al.* (1986) on low-pressure $C_2H_2/O_2/Ar$ combustion.

II EXPERIMENTAL PROFILE MEASUREMENTS

All of the temperature, velocity, mass spectrometric and optical species profiles have been obtained under identical experimental conditions in an overventilated, laminar methane/air diffusion flame burning on a Wolfhard-Parker slot burner at atmospheric pressure. Figure 1 shows a schematic diagram of this experimental burner as well as the axisymmetric burner used in the computations. In the Wolfhard-Parker geometry fuel flows from the central slot (width = 8 mm) and dry air from each of the two outside slots (width = 16 mm). This three-slot burner configuration produces two identical, two-dimensional flame sheets of length = 40-45 mm in the y direction in Fig. 1. The long pathlength of uniform temperature and composition greatly facilitates making absorption and fluorescence measurements. In addition, all of the profiles are symmetric about the burner centerline, which allows highly precise determination of lateral positions ($\pm$ 0.1 mm) in the x direction.

In order to obtain steady laminar conditions the CH_4/air flame was stabilized using a rectangular, wire screen chimney with interior gulls, similar to that described by Kent *et al.* (1981). The flame impinged upon these gulls at a height of approximately 45 mm, while profile measurements were carried out in the region from 1 to 21 mm above the burner. Temperature, velocity, and species profiles have been obtained by moving the

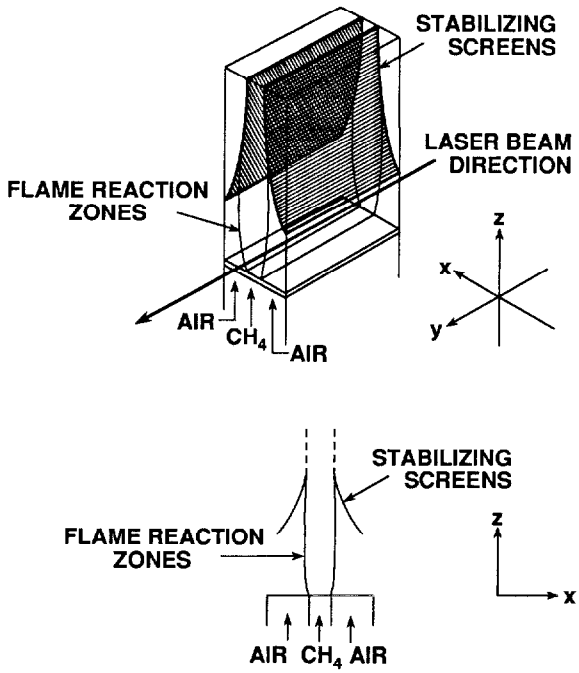

FIGURE 1 Schematic diagrams of the co-flowing two-dimensional flame geometries: the experimental Wolfhard-Parker burner and the axisymmetric configuration used in the flame structure computations. The two-dimensional views are drawn to scale in order to illustrate the different flame sizes.

burner in the lateral (x) direction at a series of heights, while keeping the thermocouple, the LDV apparatus, the mass spectrometer sampling probe, or the laser beam and associated detection optics at fixed position. The cold flow velocities for the fuel (99.9% pure methane) and the air flows were 11.0 and 21.7 cm/s, respectively. These velocities have been re-calibrated since our first paper on profile measurements (Smyth *et al.*, 1985), giving somewhat higher values.

Although measurements have been made at heights (H) from 1 to 21 mm above the burner surface, most of our data have been obtained around H = 9 mm. This has been

a convenient region in which to analyze hydrocarbon growth chemistry (Miller *et al.*, 1986; Smyth and Miller, 1987) because the concentrations of acetylenic and aromatic hydrocarbons are appreciable, yet significant amounts of soot have not yet formed (Smyth *et al.*, 1985). For the present investigation all of the experimental data have been obtained at H = 9 mm. Specific details on the experimental measurements are given in the following sections and under Results and Discussion (Section V).

A. Temperature and Velocity

Temperature profiles have been obtained with an uncoated 125 μm diameter fine wire Pt/Pt-10%Rh thermocouple (Smyth *et al.*, 1985). Corrections due to radiation were 6.2% at the highest temperatures (130 K at T = 2080 K), and the effects of catalytic heating of the thermocouple bead are expected to be small in this flame (Schoenung and Hanson, 1981; Delfau and Vovelle, 1984; Drake and Blint, 1991). In the region of H = 7, 9, and 11 mm above the burner the flame sheets are almost vertical, with the peak temperatures occurring at ± 6.3, 6.6, and 6.7 mm from the burner centerline, respectively. The thermocouple temperature measurements are estimated to be accurate to ± 5% (Smyth *et al.*, 1985, 1990).

Both the vertical and horizontal components of the convective flow velocity have been measured using laser Doppler velocimetry (Smyth *et al.*, 1985). Buoyancy dominates the velocity field within a few millimeters above the burner surface, leading to significant entrainment. Many of the streamlines exhibit trajectories which originate in the lean region of the flame (on the air side of the flame sheets), cross the high temperature, primary reaction zones, and continue into the fuel-rich regions.

B. Mass Spectrometer Measurements

Profiles of the major stable flame species (N_2, O_2, CH_4, CO_2, H_2O, CO, H_2, C_2H_2, and Ar) have been collected with a direct-sampling mass spectrometer equipped with a quartz microprobe (orifice diameter = 120-140 μm). Since our original profile data were presented (Smyth *et al.*, 1985), numerous additional measurements have been made (for example, Hamins *et al.*, 1990). All of the mass spectrometric data presented here for the stable species are from these more recent measurements. Absolute concentrations of CH_4, O_2, N_2, CO_2, H_2, C_2H_2, and Ar have been determined using a direct calibration procedure in which the species of interest was sampled from a mixture of known composition at room temperature (Smyth *et al.*, 1985). Water was calibrated against the relative humidity measured in the room air. For determining the CO concentration, mass 28 profile data were collected at three different electron energies (13, 16, and 20 eV) and the contributions from N_2 and C_2H_4 were subtracted from the total signal.

Successful profile measurements of the methyl radical $CH_3\cdot$ have also been made by using a quartz microprobe modified so that iodine vapor could be introduced into the inside of the tube (Miller and Taylor, 1987). The sampled methyl radicals react quantitatively in the tip of this scavenger probe to form methyl iodide ($CH_3\cdot + I_2 \rightarrow CH_3I + I\cdot$), which can then be detected in the mass spectrometer. These results represent an important check on possible disturbances caused by the quartz microprobe, since multiphoton ionization of the methyl radical has also been used to make profile measurements (Smyth and Taylor, 1985). Excellent agreement has been observed in both the location and the shape of the profiles for the mass spectrometric and optical measurements (Smyth and Miller, 1987), considering that the spatial resolution of the quartz microprobe [effective sampling diameter ≈ 0.7 mm (Smyth *et al.*, 1985)] is larger than that of the multiphoton ionization experiments (d ≈ 0.1 mm).

All of the mass spectrometric data have been analyzed by assuming that the observed signal intensity is proportional to the molecular flow rate through the orifice in the quartz microprobe (Smyth *et al.*, 1985). In addition, the temperature dependence of the mass flow rate ($dm_i/dt \propto T^{-0.5}$) has been taken to be that appropriate for a critical flow orifice (Fristrom and Westenberg, 1965). The errors in the absolute concentrations for the major species have been estimated to be ± 10–20% (Smyth *et al.*, 1985). In the following analysis all of the mass spectrometric profile data have been symmetrized (averaged about the burner centerline) but not otherwise smoothed.

C. *Optical Measurements*

The Wolfhard-Parker rectangular slot burner is especially well suited for making absorption measurements along the burner axis (in the y direction in Fig. 1) as well as detecting laser-induced fluorescence at 90° to the direction of the laser beam. In addition to absorption and laser-induced fluorescence measurements, multiphoton ionization has been employed for obtaining species profile data.

Laser absorption has been used to make direct quantitative concentration measurements of OH· and CO. The absolute peak OH· concentration was determined at a height H = 7 mm above the burner by measuring absorption on the $R_2(4)$, $P_1(9)$, and $P_1(12)$ lines in the (v′, v″) = (0,0) band of the $A^2\Sigma^+ \leftarrow X^2\Pi_i$ electronic system (Smyth *et al.*, 1990). These data have been used to calibrate relative laser-induced fluorescence profiles wherein OH· fluorescence was excited on the $P_1(9)$ rotational line in the (1,0) band near 286 nm and detected in the (1,1) band at 314 nm. Errors in the concentration profiles were estimated to be ≤ 10% over a dynamic range of ten. Absolute CO concentrations have recently been measured using tunable diode laser spectroscopy (Miller *et al.*, 1992). Both single beam absorption and wavelength modulation measurements have been made on the P(8), P(11), P(12), R(2), and R(11) lines of the (1,0) vibrational band. The derived profiles are in excellent agreement with our earlier mass spectrometric results.

In addition to the laser-induced fluorescence measurements on OH·, relative concentration profiles of O atoms and CH· have also been obtained using fluorescence methods. For O atoms the two-photon $2p\ ^3P \rightarrow\rightarrow 3p\ ^3P$ transition was excited at 226 nm, and fluorescence to the $3s\ ^3S$ state at 845 nm was monitored. It was found that low photon intensities ($\leq 2 \times 10^8$ W/cm^2) and a retroreflected beam, Doppler-free geometry were required in order to minimize the photolytic production of O atoms. Laser-induced fluorescence from CH· was observed by exciting the R(6) rotational lines at 427.4 nm in the (0,0) band of the $A^2\Delta - X^2\Pi_r$ electronic transition and detecting emission from the same vibronic band (Norton and Smyth, 1991). In these measurements it was necessary to use monochromator detection of the fluorescence signal at 431 nm (as opposed to narrow-band filters) in order to avoid strong interference from polycyclic aromatic hydrocarbons.

Multiphoton ionization has been utilized for the detection of H atom (Smyth and Tjossem, 1990a) and the methyl radical (Smyth and Taylor, 1985); both cases involved 2 + 1 excitation processes. The most sensitive measurements have been obtained by using a dual electrode arrangement positioned perpendicular to the direction of the laser beam (Smyth and Tjossem, 1990b), which provides a high local electric field. Excitation of the $1s \rightarrow\rightarrow 2s$ transition in H atom at 243 nm was followed by ionization via absorption of a third photon. As found for O atom, using photon intensities of $\leq 2 \times 10^8$ W/cm^2 and a retroreflected beam, Doppler-free geometry were required in order to reduce the photolytic production of H atoms in rich flame regions to acceptable levels. Methyl radical (CH_3·) has been observed by using two photons to excite the $3p\ ^2A_2''$ Rydberg state from the ground electronic state $\tilde{X}\,^2A_2''$ at 333.5 nm. New measurements made with

the dual electrode arrangement have provided profile data at higher flame positions, including H = 9 mm (Smyth and Norton, 1990), than did our earlier experiments with a single electrode (Smyth and Taylor, 1985).

Corrections for the variation in the collisional quenching rate must be included in the analysis of any profile data obtained using laser-induced fluorescence and multiphoton ionization. For these calculations the thermocouple temperature data and mass spectrometric measurements of the major species have been used, combined with available quenching cross sections (Smyth *et al.*, 1990; Smyth and Tjossem, 1990a). Since appreciable radical concentrations occur over only a limited spatial region in the CH_4/air diffusion flame, the overall effect of these quenching rate corrections is small.

An additional correction for the variation of the electron detection sensitivity as a function of flame position must be taken into account for the multiphoton ionization measurements. In contrast to the quenching corrections, this effect can be significant in diffusion flames at atmospheric pressure, due to steep temperature and ion concentration gradients (Smyth and Tjossem, 1990b). The electron detection sensitivity has been measured as a function of flame position by making two comparisons: (1) the CO ionization (2 + 1 excitation of the $B^1\Sigma^+$ state at 230 nm) and fluorescence signals ($B^1\Sigma^+ \rightarrow A^1\Pi$ emission at 484 nm) and (2) the argon 3 + 1 $3p^6 \rightarrow\rightarrow\rightarrow 3p^5 4s$ multiphoton ionization signal at 314.4 nm and mass spectrometric measurements (Smyth and Tjossem, 1990b). Relative concentration data obtained using multiphoton ionization are difficult to measure with high precision in rich flame regions due both to this correction as well as to significant ionization from hydrocarbons. Profiles have been obtained by subtraction of signals recorded with the laser tuned on and off resonance and then corrected for the electron detection sensitivity as a function of flame position.

D. Database Consistency Checks

The previous sections have summarized the methods by which extensive experimental measurements of species concentrations, temperature, and velocity have been compiled over the past seven years. These results have been examined for internal consistency in a number of ways, in order to produce a unified, comprehensive database suitable for comparison with detailed computations of diffusion flame structure. For example, application of the continuity equation revealed that the measured horizontal velocity profile needed to be corrected to satisfy $\nabla \cdot (\rho \vec{v}) = 0$. The required adjustments were approximately 60% in the lean flame region and 30% in the rich region. These values are consistent with the estimated thermophoretic corrections which are used to derive gas velocities from the LDV measurements on 1 micron diameter alumina particles (Smyth *et al.*, 1985). The corresponding corrections for the vertical velocities are 1% or less.

A second consistency check involves the calibration of the mass spectrometric measurements. Despite careful calibration procedures (see above), the sums of the mole fractions of the major species at various heights above the burner have been found to lie systematically above 1.0, typically by 10–20%. Similar deviations have also been noted by Santoro (1991) for mass spectrometer measurements in a co-flowing, axisymmetric CH_4/air diffusion flame. Such systematic errors may arise if the flow through the quartz microprobe is not well represented by the Fristrom and Westenberg (1965) analysis that has been assumed (Smyth *et al.*, 1985). For example, a more complex dependence upon the heat capacity ratio may be needed. Therefore, all of the mass spectrometer data to be presented below have been normalized to account for $\sum_i X_i \neq 1.0$. Since the optical measurements are not subject to the same systematic errors, those species profiles have not been corrected in this fashion.

The nitrogen mole fraction profile requires special treatment because it contains considerably more random noise than those of the other species and because it exhibits a

systematic excursion above the air-stream mole fraction ($X_{N_2,2} = 0.7808$) on the fuel-lean side, between lateral positions ± 7 mm to ± 10 mm. Unless some sort of correction is applied to N_2 in advance, these errors will be propagated to all other species in the normalization process to account for $\sum_i X_i \neq 1.0$. Since N_2 is nearly chemically inert under the current flame conditions, a revised N_2 profile has been derived by setting the net N_2 chemical production rate equal to zero. In Bilger's (1976) formulation, this production rate is given by

$$\omega_{N_2} = -\rho D(\nabla\xi)^2(d^2Y_{N_2}/d\xi^2) = 0,$$

where Y_{N_2} = mass fraction of N_2, ξ = mixture fraction (see Section IV), D = diffusion coefficient (see Section IV), and ρ = density. With the boundary conditions $Y_{N_2} = 0.7552$ at $\xi = 0$ and $Y_{N_2} = 0$ at $\xi = 1$, the solution is $Y_{N_2} = 0.7552\ (1\text{-}\xi)$. The resulting nitrogen mole fraction profile, obtained as $X_{N_2} = Y_{N_2}\ (W_{avg}/W_{N_2})$ where the W's denote molecular weights, appears reasonable. The calculated N_2 profile decreases smoothly and monotonically from just below the air-stream value at the lean edge of the flame to 0.13 at the centerline for H = 9 mm above the burner surface.

After this correction has been made to the N_2 profile, the proper normalization for all of the other mass spectrometric data cannot be carried out by simply using the total sum of all the measured mole fractions. N_2 and the optically detected species OH·, H atom, O atom and CH· are first excluded from the mole sum, which yields the following normalization:

$$X_{CORRECT,i} = X_{RAW,i} * \frac{[1 - (X_{N_2} + X_{optical})]}{[\sum_i X_i]},$$

where X_i represents the mole fraction of species i and i = CH_4, O_2, CO_2, H_2O, CO, H_2, C_2H_2, CH_3·, and Ar.

III FLAME STRUCTURE COMPUTATIONS

Whereas all of the experimental measurements have been made in a CH_4/air diffusion flame burning on a rectangular Wolfhard-Parker slot burner, no computations of flame structure have been carried out for this geometry due to the difficulty in specifying the downstream boundary conditions. Boundary conditions for the temperature and species concentrations cannot be measured experimentally at the position of the stabilization screen, without which the free-burning CH_4/air diffusion flame is unsteady. The closest available and most detailed 2-dimensional model calculations are those for an axisymmetric co-flowing flame (Smooke *et al.*, 1989, 1990). In addition to the geometrical differences in the experimental and computational burner configurations, the visible experimental flame height is 33 cm versus the calculated flame height of 3.8 cm (where the stoichiometric mixture fraction occurs on the centerline). It is thus important to choose a geometry-independent coordinate for the comparison of the experimental data with the computed profiles. This can be accomplished by using a conserved scalar, such as the local equivalence ratio (ϕ) or the mixture fraction (ξ); see Section IV.

The chemical structure of an unconfined, co-flowing, axisymmetric, CH_4/air diffusion flame was computed with detailed transport and finite rate chemistry. C_1 and C_2 chemistry were included in a reaction mechanism which involved 83 reversible reactions and 26 species. This is a new calculation with the same mechanism as that used by Puri *et al.* (1987; the A factor for the H· + O_2 reaction has been reduced to 2.0×10^{14} s^{-1}), with the addition of the CH· + O_2 → HCO· + O: channel plus CH· reactions with OH·, H_2O, CO_2, and CH_4. All of the rates for these additional CH· reactions have been taken from

the compilation by Miller and Bowman (1989). In the flame structure computation fuel was introduced through an inner tube with radius $R_I = 0.2$ cm, and air flowed through a co-flow tube having a radius $R_O = 2.5$ cm, which was surrounded by a zero-velocity collar with an outer radius of 10.0 cm (see Fig. 1). The boundary conditions at the inlet ($z = 0$) are given for $r < R_I$ by

$$T = 298 \text{ K}$$

$$Y_{CH_4} = 1.0,\ Y_k = 0,\ k \neq CH_4$$

$$v_r = 0.0 \text{ cm/s},\ v_z = 35.0 \text{ cm/s}$$

and for $R_I < r < R_O$ by

$$T = 298 \text{ K}$$

$$Y_{O_2} = 0.232,\ Y_{N_2} = 0.768,\ Y_k = 0,\ k \neq O_2, N_2$$

$$v_r = 0.0 \text{ cm/s},\ v_z = 35.0 \text{ cm/s},$$

where r and z are the radial and axial coordinates, respectively, Y_k is the mass fraction of species k, and v_r and v_z are the initial cold flow velocities.

The inlet boundary condition for the methane concentration is consistent with experimental mass spectrometric measurements carried out near the base of the Wolfhard-Parker flame; the CH_4 mole fraction is 1.0 at the burner centerline for a height H = 3 mm above the burner. There are some minor differences between the other boundary conditions and the experiment. The computational air composition does not include argon, which accounts for the value of $Y_{N_2} = 0.768$ used in the calculation, compared to $Y_{N_2} = 0.7552$ for the experimental analysis. In addition, the burner preheats the inlet gas flows in our experiments to 328 K. The largest difference between the experimental and computational boundary conditions involves the inlet gas flow velocities, which are much larger in the flame structure calculation. A separate computation was performed with lower exit flow velocities (17.5 cm/s vs. 35 cm/s) and no zero-velocity collar (overall outer radius 2.5 cm vs. 10.0 cm). However, this calculation was not used for the comparison with the experimental results because the computed flame covers an insufficient range of scalar dissipation rates (see Section IV). The species profiles in the two computations agree closely with one another, which shows that the calculated chemical structure is not sensitive to the inlet gas velocities.

The solution procedure employed a combination of pseudo-time integration and an adaptive finite difference method to obtain profiles for the dependent variables; the details have been presented previously (Smooke *et al.*, 1989). The elliptic form of the governing conservation equations was solved with a stream function-vorticity formulation on a two-dimensional mesh, the initial nodes of which were formed by the intersection of lines drawn in the radial and axial directions. Starting with a flame sheet estimate on an initial coarse grid, a time-dependent approach was used to help obtain a converged numerical solution. Grid points were then inserted adaptively, and the steady-state procedure was utilized to complete the computation.

IV ESTABLISHING A BASIS FOR COMPARISON OF EXPERIMENT AND MODEL PROFILES

It has become customary in recent years to present model results as functions of a geometry-independent coordinate, such as the local equivalence ratio (ϕ) or the mixture fraction (ξ). This choice has been motivated primarily by the search for a simplified

description of laminar diffusion flame chemistry for use in calculations of turbulent reacting flows (Liew *et al.*, 1984; Drake, 1986; Peters, 1984, 1986; Peters and Kee, 1987; Puri *et al.*, 1987; Bilger *et al.*, 1990; Seshadri *et al.*, 1990; Smooke *et al.*, 1990). For the purposes of validating a model by comparison with experimental data, the coordinate transformation of the independent variable from a measured laboratory distance to a derived mixture fraction is not ideal, because ξ is determined from the local species concentrations and therefore is not a truly independent variable. Despite this limitation, the mixture fraction representation remains a useful starting point as a means for comparing model results with experimental data from different burner geometries and different flame sizes, as in the current study.

A. Mixture Fraction

The mixture fraction may be defined in many different ways, all of which can be expressed in the form $\xi = (\beta\text{-}\beta_2)/(\beta_1\text{-}\beta_2)$, where β represents any linear combination of conserved scalars (quantities that vary in the flow but have no chemical sources or sinks: see Williams, 1985; Bilger, 1976; Peters, 1984) and the subscripts 1 and 2 indicate limiting values in the fuel and oxidizer streams, respectively. Thus, ξ may be considered to be a form of the equivalence ratio (ϕ), normalized such that it varies from 0 in the oxidizer stream to 1 in the fuel stream. For example, the choice of $\beta = Z_C$ (the local mass fraction of carbon atoms) produces $\xi_C = Z_C/Z_{C,1}$, while $\beta = Z_O$ gives $\xi_O = 1 - (Z_O/Z_{O,2})$.

The formulation of simplified conserved-scalar equations in laminar flamelet theory requires the assumption that a uniform diffusion coefficient D is valid for all species, which implies that all definitions of ξ should agree at each point in the flame (Williams, 1985; Bilger, 1977; Peters, 1984). In reality, each species diffuses at its own rate, and differential diffusion of heavy and light species may cause differences among the various forms of ξ. Bilger (1988) has introduced a definition of the mixture fraction derived from

$$\beta = 2(Z_C/W_C) + 0.5(Z_H/W_H) - (Z_O/W_O).$$

The subscripts C, H, and O denote the elements carbon, hydrogen, and oxygen, respectively. This description involves all of the elements which chemically react in a flame (N_2 is largely unreactive in the high temperature reaction zone [Smyth *et al.*, 1985]), and it also allows the stoichiometric surface (where $\beta = 0$ and $\xi_s = 0.055$ for the CH_4/air system) to be located accurately even in situations where the diffusion rates of individual species vary widely. Bilger's version of ξ has been chosen as the independent variable in the current study both for this reason and because its common use facilitates comparison with the results of other studies (Peters and Kee, 1987; Bilger *et al.*, 1990; Barlow *et al.*, 1990a, 1990b; Smooke *et al.*, 1990). However, it should be noted that this definition (hereafter, ξ_B) has no special features at locations other than the stoichiometric surface, x_s, and its gradient ($\nabla\xi_B$) is not immune to differential diffusion even at x_s.

The profile of ξ_B calculated from the experimental database is shown in Fig. 2 for a height of 9 mm above the burner. The location of the stoichiometric surface where $\xi_B = 0.055$ is found to be at $x_s = \pm$ 6.30 mm from the burner centerline. Four other definitions of the mixture fraction have also been examined, which include those derived from $\beta = Z_C + Z_H$ (Peters, 1984, 1986), $Z_O + Z_N$ (air), Z_C, and Z_H. At $x_s = \pm$ 6.30 mm these other versions of the mixture fraction have values within the narrow range 0.053-0.057. To express this another way, the locations of the points where $\xi_i = 0.055$ fall within $x = \pm$ 6.16 to $\pm$ 6.34 mm. At other locations the maximum deviation among these five mixture fraction profiles is 0.01. Apparently differential diffusion has only a minor effect under our experimental conditions. However, even these small differences

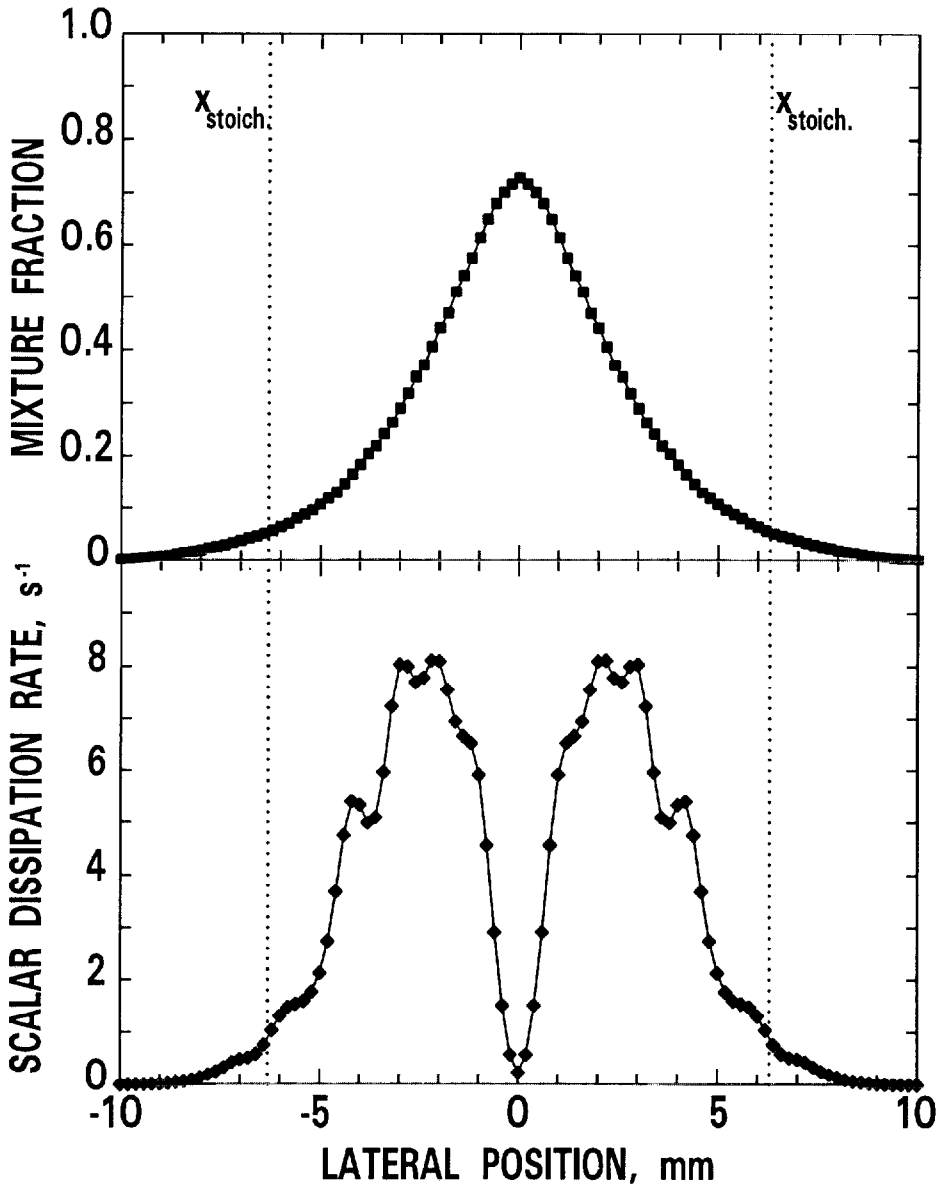

FIGURE 2 Top: experimental mixture fraction profile as a function of flame position at H = 9 mm above the burner, derived from $\beta = 2(Z_C/W_C) + 0.5(Z_H/W_H) - (Z_O/W_O)$ (Bilger, 1988). The experimental data are unsmoothed. Bottom: scalar dissipation rate as a function of flame position at H = 9 mm above the burner. Here the input mixture fraction data have been smoothed using a Savitsky-Golay filter (1964). The vertical dotted lines denote the lateral position x_s where the stoichiometric mixture fraction, $\xi_s = 0.055$.

among the ξ_i profiles can cause significant variations in quantities derived therefrom, such as the scalar dissipation rate (see below).

The calculation of the mixture fraction (by any definition) is also subject to experimental uncertainties in the measured species mole fraction profiles. If, for example, ξ_B is calculated with two different profiles of CH_4 that were measured on separate days, the values can differ by as much as 0.05 near the burner centerline. However, the value of ξ at $x = \pm 6.3$ mm changes by only 0.001; alternatively, the location of the mixture fraction at the stoichiometric surface, ξ_s, changes by only 0.04 mm. The effects of other database changes are negligible, e.g., the substitution of a CO profile measured by tunable diode laser spectroscopy instead of mass spectrometry, or the inclusion of the H atom and O atom profiles in the calculation (using estimated peak concentrations; see Section V.C.1).

There is also some uncertainty in the mixture fraction-position relationship that results from the finite spatial resolution of the experimental techniques employed. The full width of the volume sampled by the mass spectrometer probe has been estimated to be 0.7 mm (Smyth *et al.*, 1985). The resolution of the optical measurements is better, as the diameter of the laser beam is typically 0.1 to 0.2 mm at the focal spot (Smyth *et al.*, 1990; Norton and Smyth, 1991). However, the mixture fraction calculation is sensitive only to the concentrations of the major species, which have been measured by mass spectrometry. The change in mixture fraction across a distance of 0.7 mm ranges from 0.003 at the lean edges of the flame to 0.125 on the fuel-rich side between 1-2 mm from the centerline, where the $\nabla\xi$ gradient is steepest (see Fig. 2). Therefore, in plots of the experimental data against mixture fraction, the sampling range in the ξ coordinate for each data point increases steadily with increasing ξ. In the vicinity of ξ_s, this range is about $\pm$ 0.01.

B. Scalar Dissipation Rate

It has been the goal of considerable research effort to find universal state relationships for species concentrations and temperature as functions of a single variable, the mixture fraction, in order to create flamelet libraries for use in the modeling of turbulent combustion. However, despite some indications of success (Bilger, 1977; Smyth *et al.*, 1985; Saito *et al.*, 1986; Sivathanu and Faeth, 1990), it has been found in general that a second variable is needed because the supposedly universal relationships are often not observed for chemical intermediates (Smyth *et al.*, 1985; Saito *et al.*, 1986) and species concentrations can vary with the local stretch or strain rate in a flame (Drake, 1986; Peters, 1986; Seshadri *et al.*, 1990). The same is true in the current experimental and modeling results, as will be shown below. Therefore, both the mixture fraction and at least one additional variable, such as the strain rate, must be matched in some fashion if the comparison of experimental and computational data sets is to be meaningful.

The strain rate can be characterized conveniently by the scalar dissipation rate (χ), which is a function of the mixture fraction gradient: $\chi = 2D(\nabla\xi) \cdot (\nabla\xi)$ (Williams, 1985). Here D represents a diffusion coefficient that is assumed in laminar flamelet theory to be the same for all species. It has been approximated variously as:

$$
\begin{aligned}
D &\simeq 1.786 \times 10^{-5}\ T^{1.662}\ \text{cm}^2/\text{s (Bilger, 1977)},\\
D &\simeq 1.523 \times 10^{-5}\ T^{1.67}\ \text{cm}^2/\text{s (Mitchell, 1979), and}\\
D &= \lambda/\rho c_p\ \text{Le}\\
&\simeq \lambda/\rho c_p = (2.58 \times 10^{-4}/\rho)\ (T/298)^{0.7}\ \text{cm}^2/\text{s (Smooke, 1991)}\\
&= (3.92 \times 10^{-4}\ /\ W_{avg})\ T^{1.7}\ \text{cm}^2/\text{s for P = 1 atm.}
\end{aligned}
$$

Diffusion coefficients for various flame species have been calculated from our experimental concentration and temperature measurements (Miller *et al.*, 1986). Of the three

definitions of D listed above, Bilger's version most closely approximates the shape and peak magnitudes of the experimental diffusion coefficient profiles for several of the major species (N_2, O_2, CH_4) and will therefore be used in the current analysis. The definition $D = \lambda/\rho c_p$ is consistent with the assumption of the Lewis number Le = 1, but involves division by the average molecular weight, a factor which does not appear in fundamental descriptions of either binary or multicomponent diffusion coefficients (Hirschfelder *et al.*, 1954; Kee *et al.*, 1983).

For a two-dimensional system such as the Wolfhard-Parker burner used in the current experiments, the scalar dissipation rate is calculated as $\chi = 2D[(\partial\xi/\partial x)^2 + (\partial\xi/\partial z)^2]$. The horizontal gradient of mixture fraction can be determined from any of the various mixture fraction definitions discussed in Section IV.A, while the vertical gradient is obtained by comparing the corresponding mixture fraction profiles at different heights (H) above the burner. In order to avoid excessively noisy scalar dissipation rate profiles, some smoothing of the raw mixture fraction data is required (Savitzky and Golay, 1964; Miller *et al.*, 1986). In general, the $(\partial\xi/\partial z)^2$ term contributes less than 10% of the χ value, except in the highly strained part of the flame near the burner surface, and near the centerline at all heights. The profile of χ calculated from the experimental database with $\xi = \xi_B$ for H = 9 mm is shown in Fig. 2. For increasing heights above the burner, χ generally becomes smaller as concentration gradients decrease. However, χ increases with height on the lean edges of the flame, outside of x = ± 7.2 mm.

The scalar dissipation rate has also been calculated at each node in the computational grid for the modeled flame. Although diffusion coefficients for each species are determined in the flame structure computation, a single value is used for evaluating the scalar dissipation rate (see above). As in the experiments, χ decreases with increasing height above the burner. However, the correspondence between χ and height is different in the model and in the experiment because of the differences in burner geometries and flame sizes. In this situation Seshadri *et al.* (1990) have suggested that experimental data should be compared against model results for the axial location where the stoichiometric value of χ, denoted χ_s, rather than the height above the burner, matches that of the experiment.

The value of χ for the stoichiometric position at H = 9 mm is found to be 0.90 s^{-1}, if Bilger's version of ξ is used and if the diffusion coefficient is defined as $D = 1.786 \times 10^{-5}\ T^{1.662}$. If the alternate definition of $D = \lambda/\rho c_p = (2.58 \times 10^{-4}/\rho)\ (T/298)^{0.7}$ cm^2/s is employed (Smooke, 1991), χ_s becomes 0.96 s^{-1}. (Note that both of these results are lower than the value χ_s = 1.4 s^{-1} calculated from the 1985 data for this same flame position by Seshadri *et al.* (1990).) The χ_s results are generally insensitive to the degree of smoothing performed on the ξ profile before $\nabla\xi$ is calculated (uncertainties of less than ± 5%). However, if different definitions of the mixture fraction profile are utilized, the value of χ at $x_s = \pm 6.3$ mm varies quite widely between 0.46 s^{-1} (using ξ_H) and 1.44 s^{-1} (using ξ_C). Clearly it is important to use the same definitions of ξ and of D in the calculation of χ for both the model and the experiment. The computed axial position having χ_s = 0.90 s^{-1} is located at z = 5.1 mm above the burner.

An alternative suggestion has been made by Liew *et al.* (1984) that the computational axial location for comparison with experimental data should be selected on the basis of matching values of χ at T_{max}, rather than χ at the stoichiometric flame position x_s. If this is done for the current experimental data set, the best match for the scalar dissipation rate is at χ = 0.58 s^{-1}, which corresponds to z = 11.4 mm above the burner in the computed flame, i.e. a more "relaxed" region of the flowfield.

We have found that matching values of χ at a single point, whether it be x_s or T_{max}, is unsatisfactory because the profiles of χ do not vary smoothly or monotonically, even in the computed case, and especially not in the vicinity of the stoichiometric position and

the peak temperature (see Fig. 2). Rather, it is important to match the experimental and calculated profiles of χ across the full range of mixture fractions that are to be considered in the species profile comparisons. In the current study this match has been optimized by finding the computational axial location for which the sum of the squares of the fractional differences between the values of χ in the model and in the experiment is minimized over the range of mixture fraction from $\xi = 0.0$ to $\xi = 0.20$. This procedure selects the same axial location from the computational results if the mixture fraction range is reduced to $\xi = 0.02$ to 0.09. However, if the mixture fraction range is reduced further around the stoichiometric value of $\xi_s = 0.055$, the best matched axial location is found to be somewhat lower in the computed flame. Following the procedure outlined above, the best match for the experimental data obtained at H = 9 mm above the burner is the axial location that corresponds to a height z = 7.7 mm in the modeled flame.

In order to illustrate the extent to which the model results vary with height above the burner and with the local strain rate, each comparison figure for the species concentrations and the temperature shown below includes the computational results not only from the best matched axial location, but also for the location having χ_s values approximately 2.5 times larger and smaller. For the best matched axial location the scalar dissipation rate at the stoichiometric flame position, χ_s, is 0.63 s^{-1}, compared to the experimental value of 0.90 s^{-1} at H = 9 mm. At the higher strain rate location the computed χ_s is 1.5 s^{-1}, and for the lower strain rate position χ_s is 0.26 s^{-1}. Figure 3 shows the experimental scalar dissipation rate as a function of the mixture fraction and the calculated profiles for these three axial locations, which span a region in the computed flame from a height of z = 3.2 mm to z = 17.4 mm. This range of model results easily encompasses both of the locations that would have been chosen on the basis of matching χ at either x_s or T_{max}.

TABLE I

Experimental peak temperatures, location of T_{max}, location of the stoichiometric surface, and the scalar dissipation rate as a function of height in the CH_4/air flame burning on a Wolfhard-Parker burner.

Height Above Burner (mm)	Peak Temperature (K)	Spatial Location of T_{max} (mm)	Spatial Location of Stoichiometric Surface x_s (mm)	Scalar Dissipation Rate χ_s, (s^{-1})
11	2109	±6.7	±6.46	0.44
9	2080	±6.6	±6.30	0.90
7	2053	±6.3	±6.16	1.37

In the next section the calculated species and temperature profiles are presented along the radial coordinate at specific axial locations. For both the experimental measurements and the computed flame structure, carrying out the data analysis along horizontal trajectories is essentially identical to examining the profiles along a path normal to lines of constant mixture fraction. This is true because the experimental and computed flames have closely similar shapes in the region of comparison. The experimental locations of the stoichiometric surface (x_s) are ± 6.16, ± 6.30, and ± 6.46 mm at H = 7, 9, and 11 mm, respectively, and the corresponding values of χ_s are 1.37, 0.90, and 0.44 s^{-1}. These results are summarized in Table I and show that the flame sheets bow out slightly, while χ_s decreases rapidly, with increasing height above the burner. In the computed flame similar trends occur in the region which is best matched in terms of the scalar dissipation rate. The radial location of T_{max} increases slowly, and χ_s decreases slowly with increasing height above the burner. Despite its small physical size, the computed axisymmetric flame exhibits a considerably smaller rate of change of the scalar dissipation rate (i.e., curvature) than does the larger experimental flame.

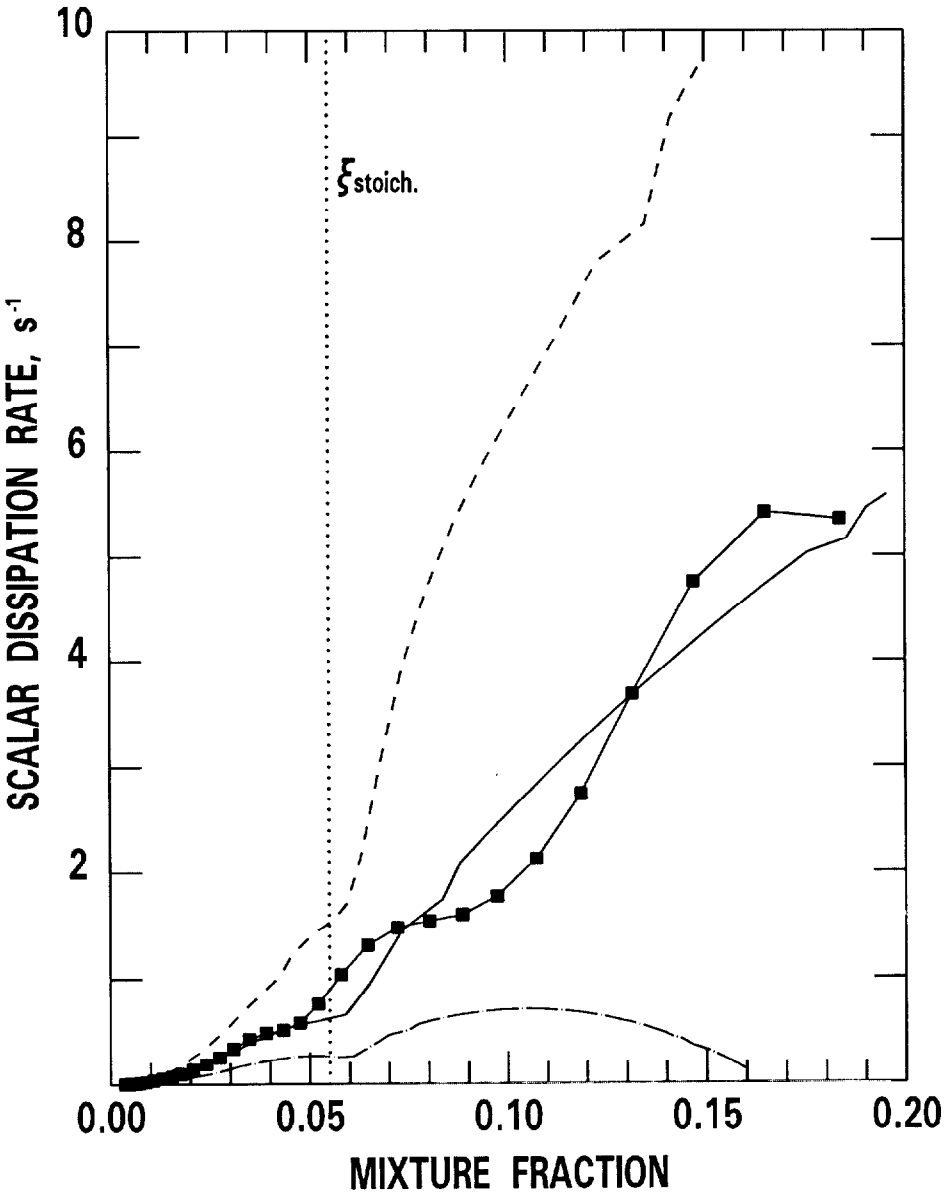

FIGURE 3 Scalar dissipation rate versus mixture fraction; the experimental data at H = 9 mm above the burner are shown as solid squares (■, χ_s = 0.90 s^{-1}), while the best matched axial location over a range of mixture fraction from the flame structure computation is drawn as a solid line (χ_s = 0.63 s^{-1}). The scalar dissipation rate curves are also shown for the higher strain rate (χ_s = 1.5 s^{-1}, dashed line) and the lower strain rate (χ_s = 0.26 s^{-1}, dash-dot line) cases which are used in the subsequent figures. The vertical dotted line denotes the location of the stoichiometric mixture fraction, ξ_s = 0.055.

V RESULTS AND DISCUSSION

A. *Temperature*

The computed adiabatic flame temperature for a methane/air mixture burning at stoichiometric conditions is 2225 K (Smyth *et al.*, 1985). Since heat is lost by convection and radiation in a diffusion flame, one expects that the experimental and calculated peak temperatures will be somewhat lower. Figure 4 shows that this is indeed the case but also that our radiation-corrected thermocouple measurements and the computational results differ significantly. At a height of 9 mm above the burner the experimental temperature maximum is 2080 K, and this occurs just to the lean side of the stoichiometric mixture fraction (ξ_s). In contrast, the calculated temperature profile, which does not take into account any radiation losses, exhibits a peak value of 2008 K on the rich side of ξ_s. A portion of the temperature disagreement can be attributed to preheating of the air and fuel streams by the burner by 30 K in the experimental measurements (Smyth *et al.*, 1985), which is not included in the calculation. Nevertheless, the difference in the location of the maximum temperatures for the measured and computed results is surprising in light of the generally good agreement found for the species profiles, including radicals (see below).

Catalytic heating is a potential concern for thermocouple temperature measurements in hydrocarbon flames. For example, Madson and Theby (1984) observed large differences at the highest temperatures between coated and uncoated thermocouples in a premixed $CH_4/O_2/Ar$ flame. However, Schoenung and Hanson (1981) reported no differences in the downstream region of a premixed CH_4/air flame for $\phi = 0.8$-1.3, and Delfau and Vovelle (1984) found similar agreement for rich ($\phi = 1.8$-3.0) C_2H_2/O_2 flames. Drake and Blint (1991) found no appreciable catalytic heating for nitrogen-diluted CH_4/air diffusion flames.

Since the thermocouple temperatures are fundamental input for our determination of species mole fractions from both the optical and mass spectrometric measurements, these data have also been checked against three optical temperature results. Laser absorption experiments on OH· have been carried out at H = 7 mm to determine populations for several individual rotational levels (Smyth *et al.*, 1990). The corresponding temperature was found to be 2080 ± 75 K, in excellent agreement with the thermocouple value of 2053 K at the same flame location. More recently, OH· rotational temperatures have been determined in our flame using laser-induced fluorescence from the S_{21} branch of the $A^2\Sigma^+ \leftarrow X^2\Pi_i$ (1,0) band, as recommended by Lawitski *et al.* (1990). Our data exhibit high precision (typically ± 40 K), but the temperature accuracy suffers from sensitivity to small baseline corrections. Nevertheless, both the peak temperature values and their location at H = 3 mm above the burner agree well with the thermocouple data. Finally, CO vibrational temperatures have been measured at H = 9 mm above the burner using tunable diode laser spectroscopy (Miller *et al.*, 1992). Again, the peak temperature result and its spatial location in the flame agree with the thermocouple temperature profile.

Several stretched laminar flame calculations of temperature profiles have been reported in counterflow CH_4/air flames (Dreier *et al.*, 1986; Puri *et al.*, 1987; Bilger *et al.*, 1990; Sick *et al.*, 1990; Barlow *et al.*, 1990, 1991). Peak temperatures are found to be near 2000 K and occur close to the stoichiometric mixture fraction, typically just on the rich side. Thermal conductivity of the mixture, convection, and the effects of finite rate chemistry account for peak temperatures below the adiabatic value; no molecular radiation losses have been included. In the work of Dreier *et al.* (1986) and Sick *et al.* (1990) the peak experimental temperature was located on the rich side of the calculated maximum value. Smooke *et al.* (1989) have also compared experimental and computed temperatures in

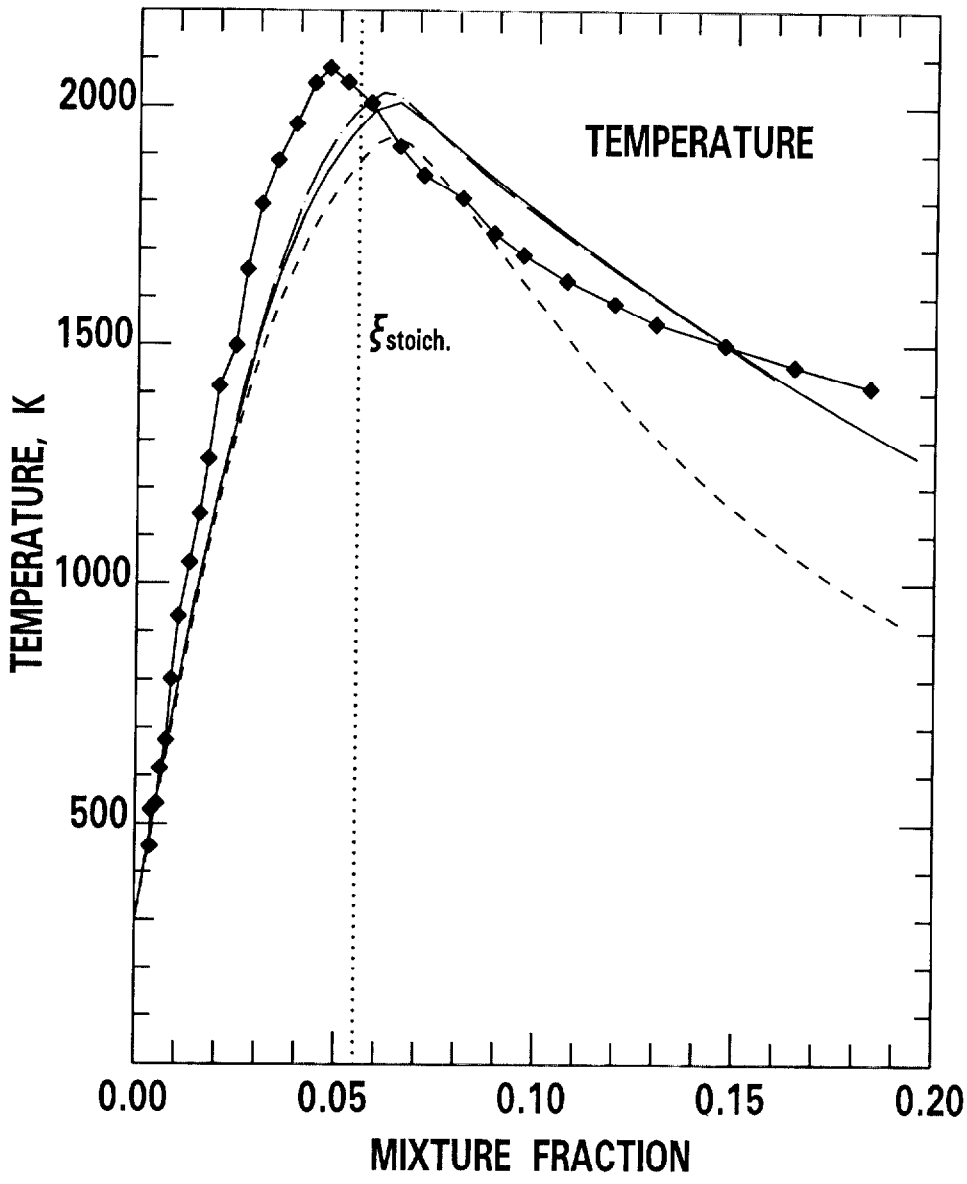

FIGURE 4 Radiation-corrected thermocouple temperature measurements (Smyth *et al.*, 1985, ♦) versus flame structure calculations; the computations are presented for three values of the scalar dissipation rate at the stoichiometric surface: $\chi_s = 0.26\ s^{-1}$ (dash-dot line), $\chi_s = 0.63\ s^{-1}$ (solid line), and $\chi_s = 1.5\ s^{-1}$ (dashed line). The vertical dotted line denotes the location of the stoichiometric mixture fraction, $\xi_s = 0.055$.

an axisymmetric, confined, co-flowing CH_4/air flame with a height of several centimeters. Good agreement in both the location and the peak temperature values was found at z = 12 mm above the burner, but at z = 24 mm the computed location of T_{max} was actually on the lean side of the experimental thermocouple data. Seshadri *et al.* (1990) compared laminar flamelet calculations of the temperature field with our experimental data. Their results are similar to Fig. 4, with the computed T_{max} (1850-1900 K) being lower than the experimental value and occurring in a richer flame region. The low T_{max} predictions have been attributed, at least in part, to simplified transport approximations (Peters, 1990).

A number of other thermocouple temperature measurements have been made in CH_4/air diffusion flames, all of which report peak temperatures in the range 2000-2060 K (Melvin and Moss, 1975; Mitchell *et al.*, 1980; Farrow *et al.*, 1982; Faris and Byer, 1987; Calcote *et al.*, 1988; Smooke *et al.*, 1989; Syed *et al.*, 1990). Faris and Byer (1987) found good agreement for the peak temperature with beam deflection tomography values, while the CARS measurements of Farrow *et al.* (1982) were lower by 70 K. In the latter study the flame location of T_{max} was identical for the CARS and the thermocouple data. Two studies also provide information on the local equivalence ratio (ϕ) or the local mixture fraction (ξ). Mitchell *et al.* (1980) found that peak temperatures occurred at $\phi = 1.0$. Syed *et al.* (1990) report that the maximum temperature lies on the lean side of ξ_s at H = 10 mm above the burner (in agreement with our results), while at higher flame positions T_{max} occurs at ξ_s.

It is also of interest to compare the location of T_{max} and the peak OH· concentration. Our experimental results at H = 9 mm show that these occur at the same lateral flame position, while our calculated position of the maximum OH· concentration lies considerably to the lean side of the computed position for T_{max}. However, at lower flame heights ($H \leq 7$ mm) where the local strain rate is higher, the experimental peak OH· concentration does lie on the lean side of T_{max} (see Section V.C.1). Melvin and Moss (1975) found that $[OH\cdot]_{max}$ and T_{max} occur at the same location in a diluted (50% N_2) CH_4/air flame at H = 5 mm above the burner. Sick *et al.* (1990) report identical $[OH\cdot]_{max}$ and T_{max} locations in an undiluted CH_4/air counterflow diffusion flame with a strain rate of 125 s^{-1}. The experimental results of Barlow *et al.* (1990a) show that $[OH\cdot]_{max}$ and T_{max} (the latter determined from Rayleigh measurements) occur at the same lean mixture fraction location in low Reynolds number turbulent CH_4/air diffusion flames diluted with 67% N_2. As found in the present study, their strained laminar flame calculations show T_{max} occurring on the rich side of their experimental temperature data. For transitional CH_4/air flames diluted with 75% air Barlow *et al.* (1991) observed that the largest OH· concentrations lie just to the lean side of the highest measured temperatures.

In summary, the available checks of thermocouple temperature measurements which have been reported in atmospheric-pressure CH_4/air diffusion flames indicate that the thermocouple data are reliable. At this point none of these results challenge our assessment that our thermocouple temperatures should be accurate to ± 5%. Therefore, the significant discrepancy between the experimental and computed temperature profiles shown in Fig. 4 remains unresolved.

B. Stable Species

Figures 5-7 compare our mass spectrometric and tunable diode laser data on the major stable species with three calculated profiles, which include the best matched axial location in terms of the scalar dissipation rate (see Section IV.B) as well as regions of higher and lower strain rate. In general the model results are more sensitive to changes in χ than

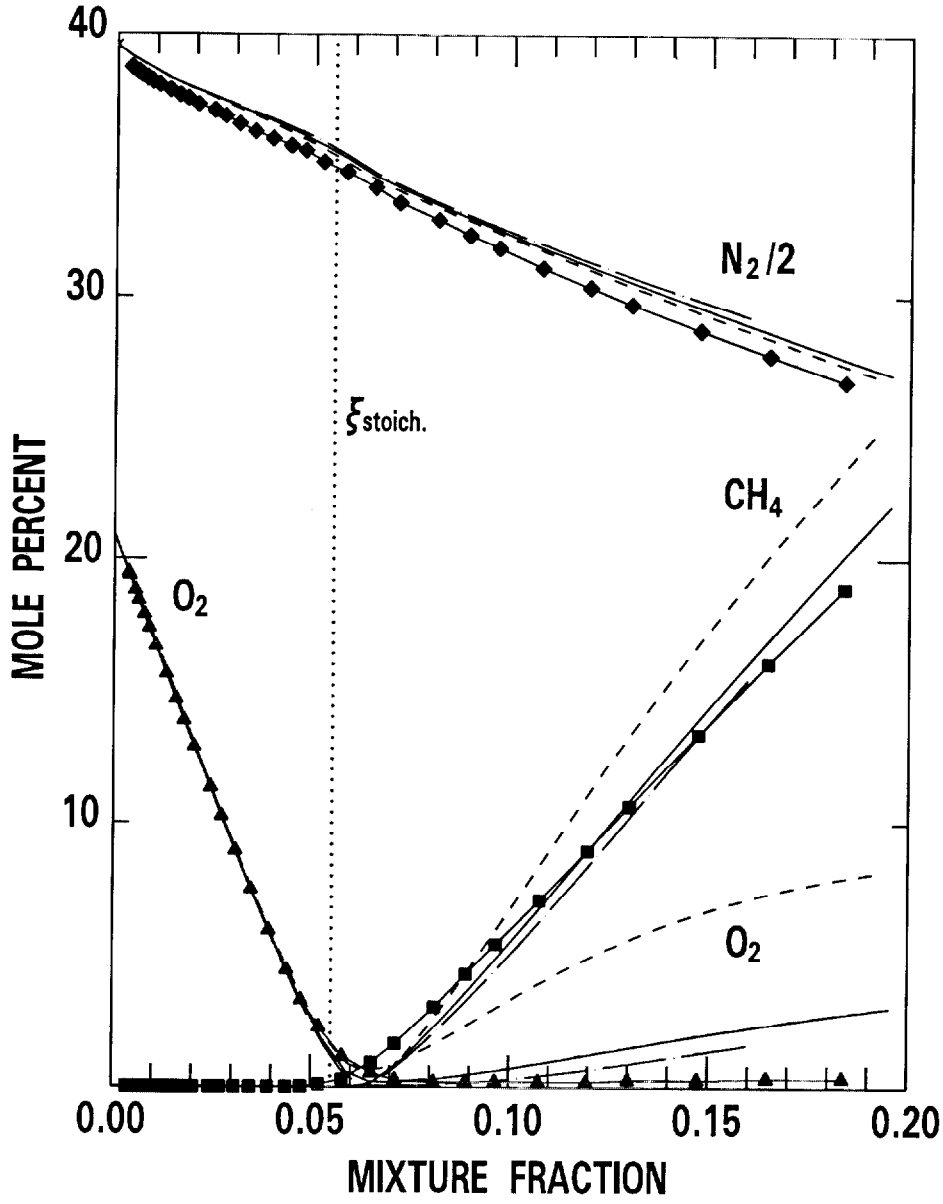

FIGURE 5 Quantitative mass spectrometric measurements of N_2 (divided by 2; ♦), O_2 (▲), and CH_4 (■) versus flame structure calculations; the computations are presented for three values of the scalar dissipation rate at the stoichiometric surface: $\chi_s = 0.26\ s^{-1}$ (dash-dot line), $\chi_s = 0.63\ s^{-1}$ (solid line), and $\chi_s = 1.5\ s^{-1}$ (dashed line). The vertical dotted line denotes the location of the stoichiometric mixture fraction, $\xi_s = 0.055$. For N_2 the experimental data points lie 1.7% below the computed values due to different definitions of the N_2 mass fraction in air (see text).

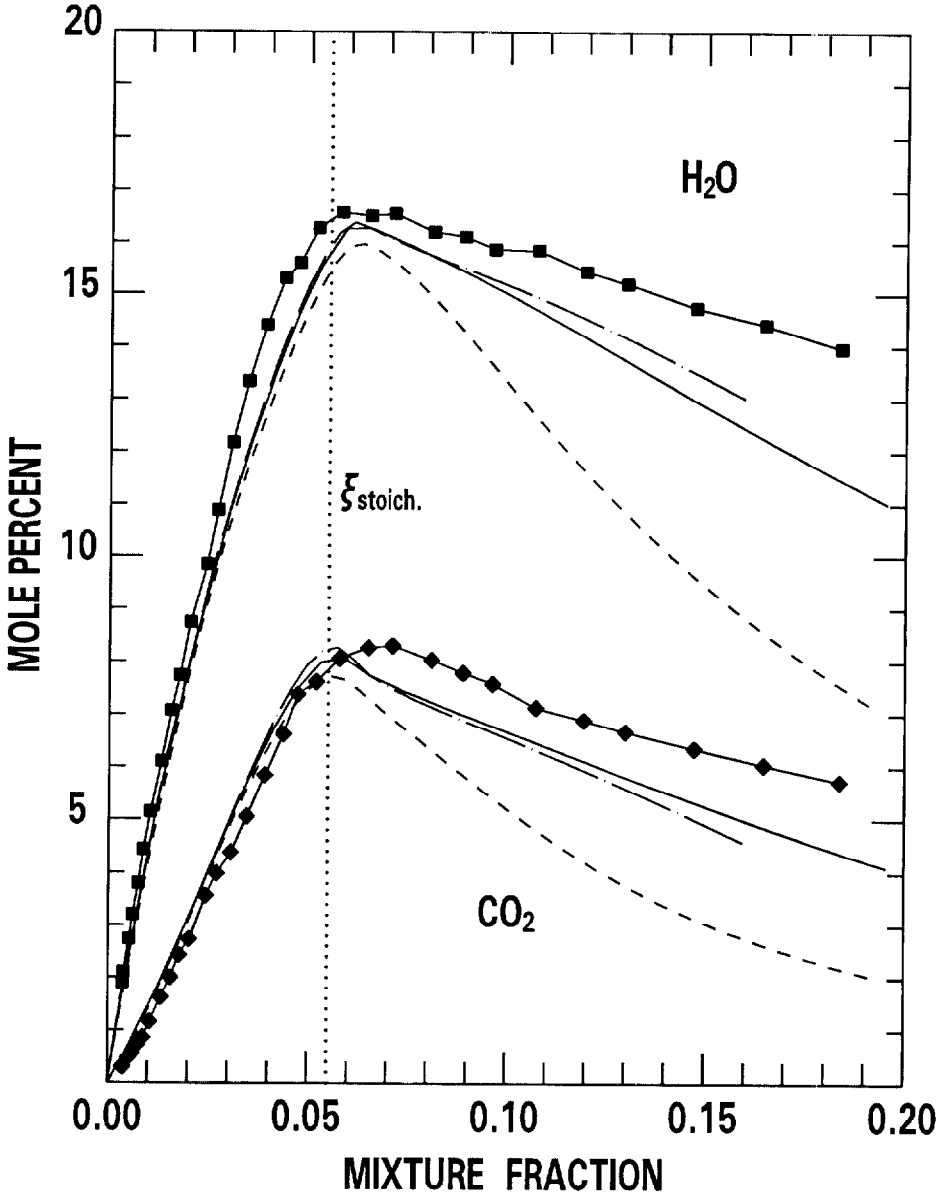

FIGURE 6 Quantitative mass spectrometric measurements of H_2O (■) and CO_2 (◆) versus flame structure calculations; the computations are presented for three values of the scalar dissipation rate at the stoichiometric surface: $\chi_s = 0.26\ s^{-1}$ (dash-dot line), $\chi_s = 0.63\ s^{-1}$ (solid line), and $\chi_s = 1.5\ s^{-1}$ (dashed line). The vertical dotted line denotes the location of the stoichiometric mixture fraction, $\xi_s = 0.055$.

are the experimental data over the range of χ considered here. Only for χ_s smaller than approximately $0.7\ s^{-1}$ do the calculated concentrations approach common values as a function of the local mixture fraction, whereas the experimental concentrations of the major species collapse onto a single curve for data obtained over a wide range of flame

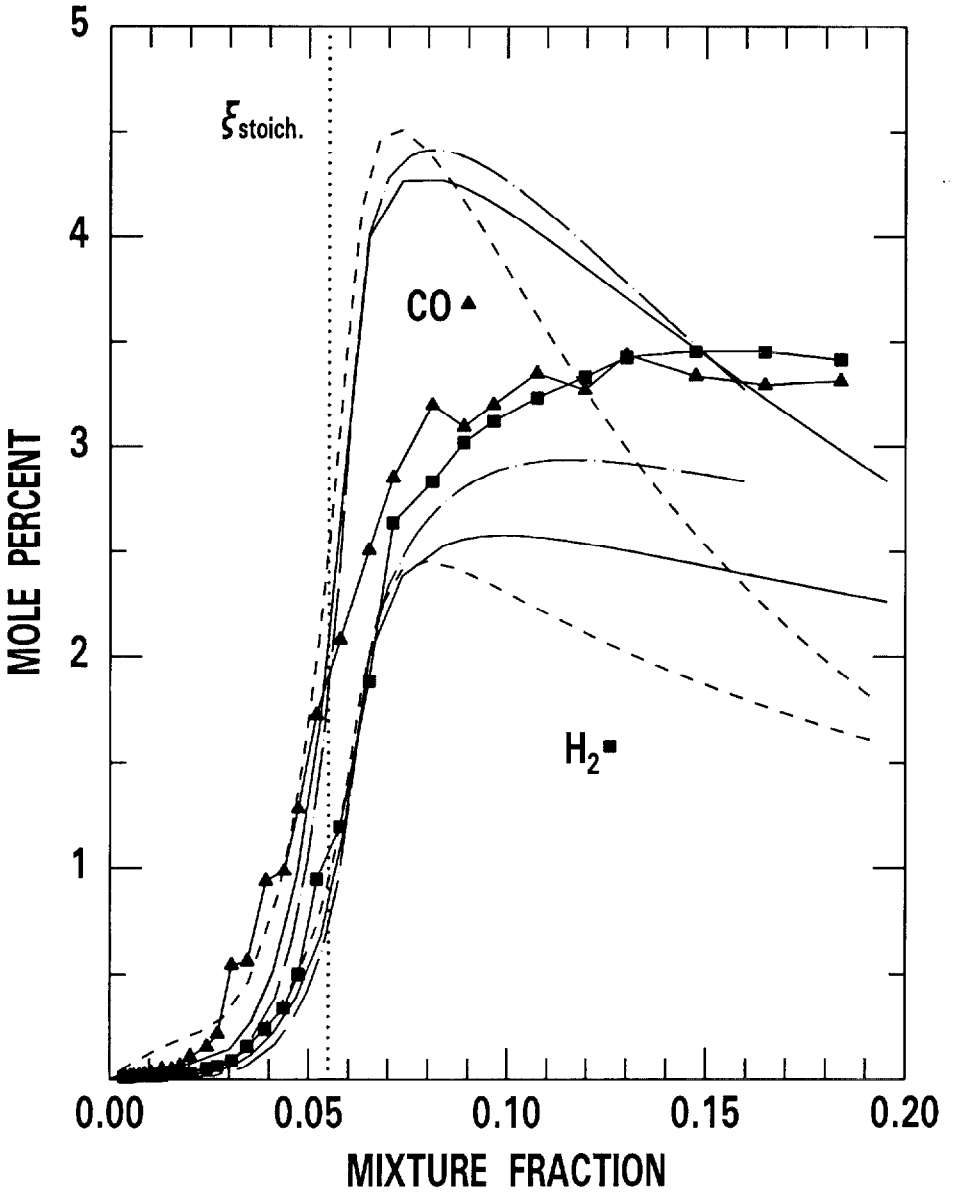

FIGURE 7 Quantitative mass spectrometric measurements of H_2 (■) and tunable diode laser measurements of CO (▲) versus flame structure calculations; the computations are presented for three values of the scalar dissipation rate at the stoichiometric surface: $\chi_s = 0.26\ s^{-1}$ (dash-dot line), $\chi_s = 0.63\ s^{-1}$ (solid line), and $\chi_s = 1.5\ s^{-1}$ (dashed line). The vertical dotted line denotes the location of the stoichiometric mixture fraction, $\xi_s = 0.055$.

heights, H = 4-16 mm (Smyth *et al.*, 1985), corresponding to scalar dissipation rates at the stoichiometric surface up to at least 2 s^{-1}.

For H_2O, CO_2, N_2, and CH_4 the experimental and computed results agree well in

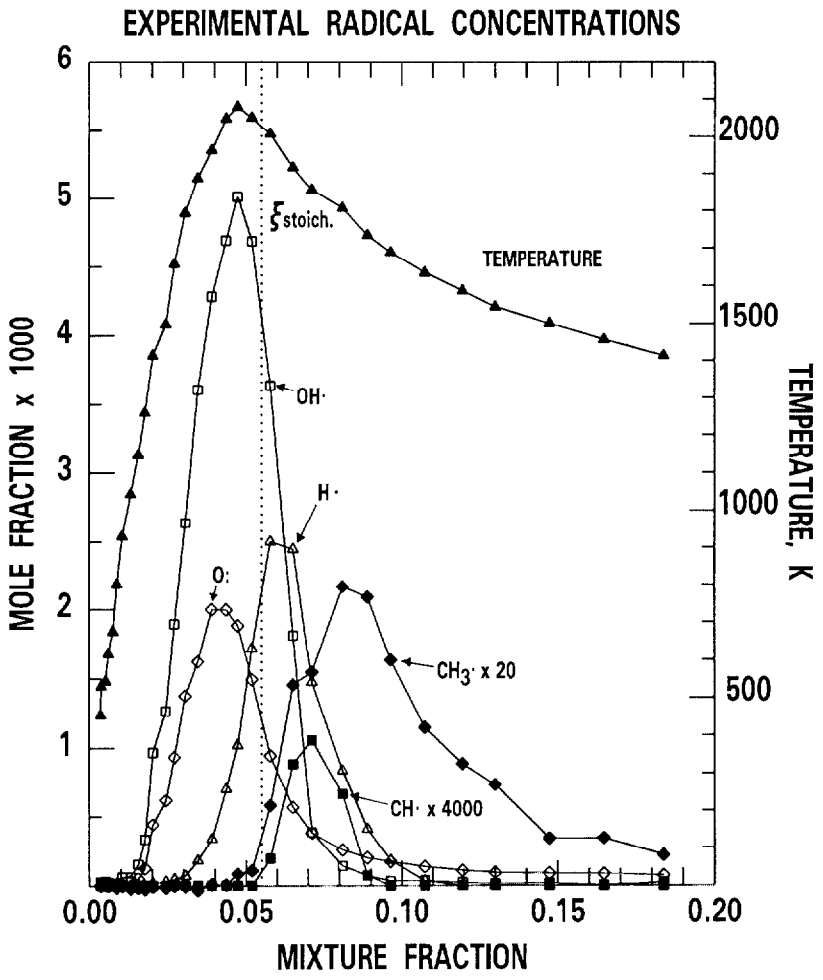

FIGURE 8a Summary of experimental results for the temperature (▲) and five radicals as a function of the mixture fraction: O atom (◇), OH· (□), H atom (△) CH· (■), and CH_3· (◆). The experimental measurements are presented for a height of 9 mm above the burner, and the computed profiles are for the best matched axial location (see text). The vertical dotted line denotes the location of the stoichiometric mixture fraction, $\xi_s = 0.055$.

terms of their absolute concentrations, the locations of their peak concentrations when plotted versus the local mixture fraction, and the shape of the profiles. The largest relative differences occur for H_2 and CO, where the measured H_2 concentration is larger than the calculated values for stoichiometric and rich conditions and the measured CO concentration is smaller for most of the rich flame region. O_2 is especially interesting. Almost exact agreement is obtained between the experimental and computed profiles for lean and stoichiometric conditions, but the calculated concentrations are much larger than the experimental values in the rich flame region. The flame structure computation exhibits no appreciable burning in at least the first 1.5 mm above the burner ($T_{max} <$ 900 K). This cold region allows significant O_2 penetration and is apparently much larger than in the experiment.

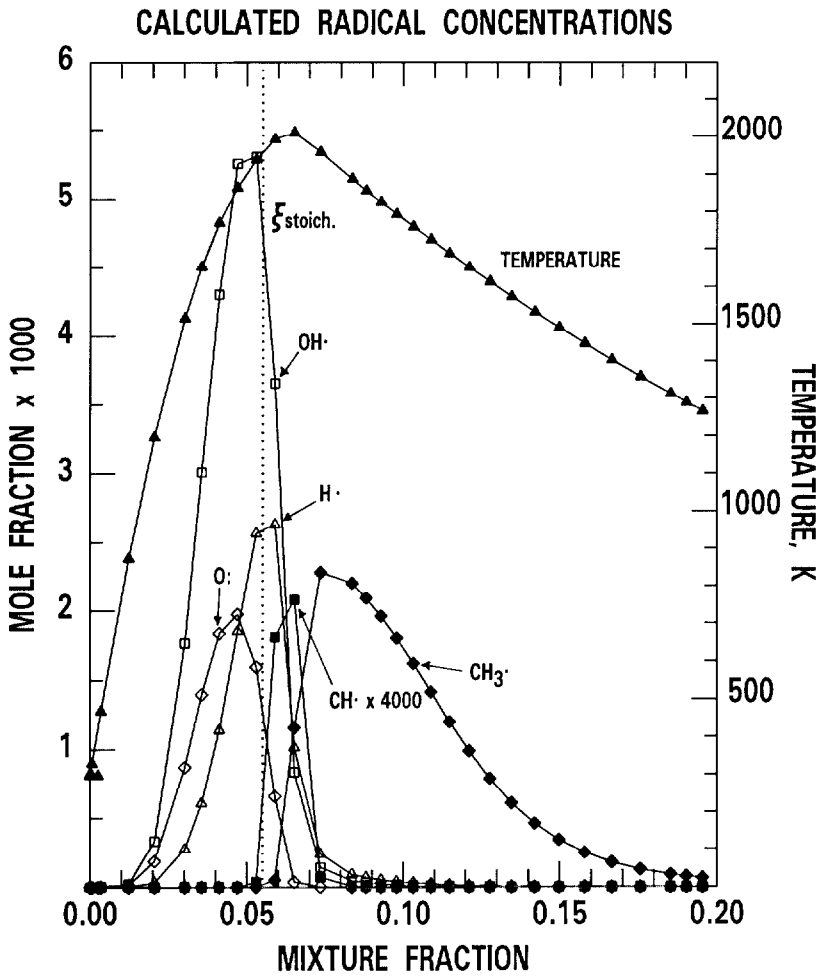

FIGURE 8b Summary of computed results for the temperature (▲) and five radicals as a function of the mixture fraction: O atom (◇), OH· (□), H atom (△) CH· (■), and CH_3· (◆). The experimental measurements are presented for a height of 9 mm above the burner, and the computed profiles are for the best matched axial location (see text). The vertical dotted line denotes the location of the stoichiometric mixture fraction, $\xi_s = 0.055$.

The chemical effects of increased O_2 penetration in the flame structure computation are difficult to evaluate. However, these are likely to be small, based upon an examination of additional axisymmetric flame structure computations. A calculation with lower exit flow velocities (17.5 cm/s) exhibited relatively more O_2 penetration than in the current calculation with v = 35 cm/s. Nevertheless, the results for the radical species profiles closely agreed with the present flame structure computation. Differences between other species profiles in these two flame structure computations can be attributed more to the effect of the extra fuel rich O_2 levels on the mixture fraction and scalar dissipation rate fields in the lower velocity case (i.e., to a change in the axial location selected by the χ-matching procedure) than to changes in specific chemical reaction rates.

C. *Radical Species*

Figure 8 compares the experimental data on five radical species with the computational results. The overall agreement in the shape and the location of the profiles is excellent, with peak concentration positions appearing in the order O atom, OH·, H atom, CH·, and CH_3· going from lean to rich mixture fractions. The experimental locations of the maximum concentrations are slightly more spread out than the calculated positions. Specific points for each radical are discussed in the following paragraphs.

1. OH·, H atom, and O atom

The combined laser absorption and laser-induced fluorescence measurements on OH· yield absolute concentration profile data which are believed to be accurate to $\leq \pm 10\%$ over a dynamic range of ten (Smyth *et al.*, 1990). The experimental peak concentration (Fig. 9) lies above the full equilibrium value and below a partial equilibrium estimate, by more than a factor of two in each case (Smyth *et al.*, 1990). These results are expected on the basis of detailed experimental measurements carried out in low pressure, premixed flames by Biordi *et al.* (1977) and Bittner (1981).

Figure 9 shows that the computed OH· profiles exhibit peak concentrations which are much closer to the experimental result than are either the full equilibrium or partial equilibrium estimates. The computed profiles are a little narrower than the experimental measurements; otherwise the agreement is excellent for the peak concentration ($1.8 \pm 0.2 \times 10^{16}$ cm^{-3} or mole fraction $= 5.0 \times 10^{-3}$) and for the peak location in terms of the local mixture fraction. In addition, our experimental results show little variation in the peak OH· concentration with flame height (Smyth *et al.*, 1985), while the calculated profiles are also relatively insensitive to the flame height, and thus to the local strain and scalar dissipation rates.

For both the H atom and O atom measurements only relative concentration profiles were obtained, since multiphoton excitation methods were utilized in their detection (Smyth and Tjossem, 1990a). Special care was taken in these experiments to avoid the photolytic production of the species of interest. Conditions were obtained for the H-atom measurements which yielded profiles showing little variation with laser intensity and thus negligible photolysis interferences. The peak H-atom concentration has been estimated from our analysis of partial equilibrium in this flame (Smyth *et al.*, 1990), which shows that the fast bimolecular reaction (usually designated R3)

$$\mathrm{OH}\cdot + \mathrm{H_2} \rightleftarrows \mathrm{H_2O} + \mathrm{H}\cdot \qquad \text{(R3)}$$

is equilibrated. This reaction controls the peak H-atom concentration in the primary reaction zone and may be used to place the experimental relative H-atom profile on an absolute basis using the species concentration data on H_2, H_2O, and OH· combined with the temperature measurements. The resulting peak H-atom concentration is 2.5×10^{-3} mole fraction, which is approximately 20 times the full equilibrium value. Figure 10 presents the experimental H-atom profile results scaled to this R3 prediction and corrected for the significant variation in the electron detection sensitivity as a function of flame position. Good agreement with the computed peak H-atom concentration is obtained, as well as with the shape of the profile. The calculated results are shifted toward slightly leaner flame positions compared to the experimental data.

The unwanted photolytic production of O atoms was the primary obstacle for determining accurate relative profiles, as in the H-atom experiments (Smyth and Tjossem, 1990a). Despite using low laser intensities and the Doppler-free approach with retroreflection of the laser beam, the photolytic production of O atoms could not be entirely eliminated. Our measurements revealed that laser-induced production of O atoms occurred

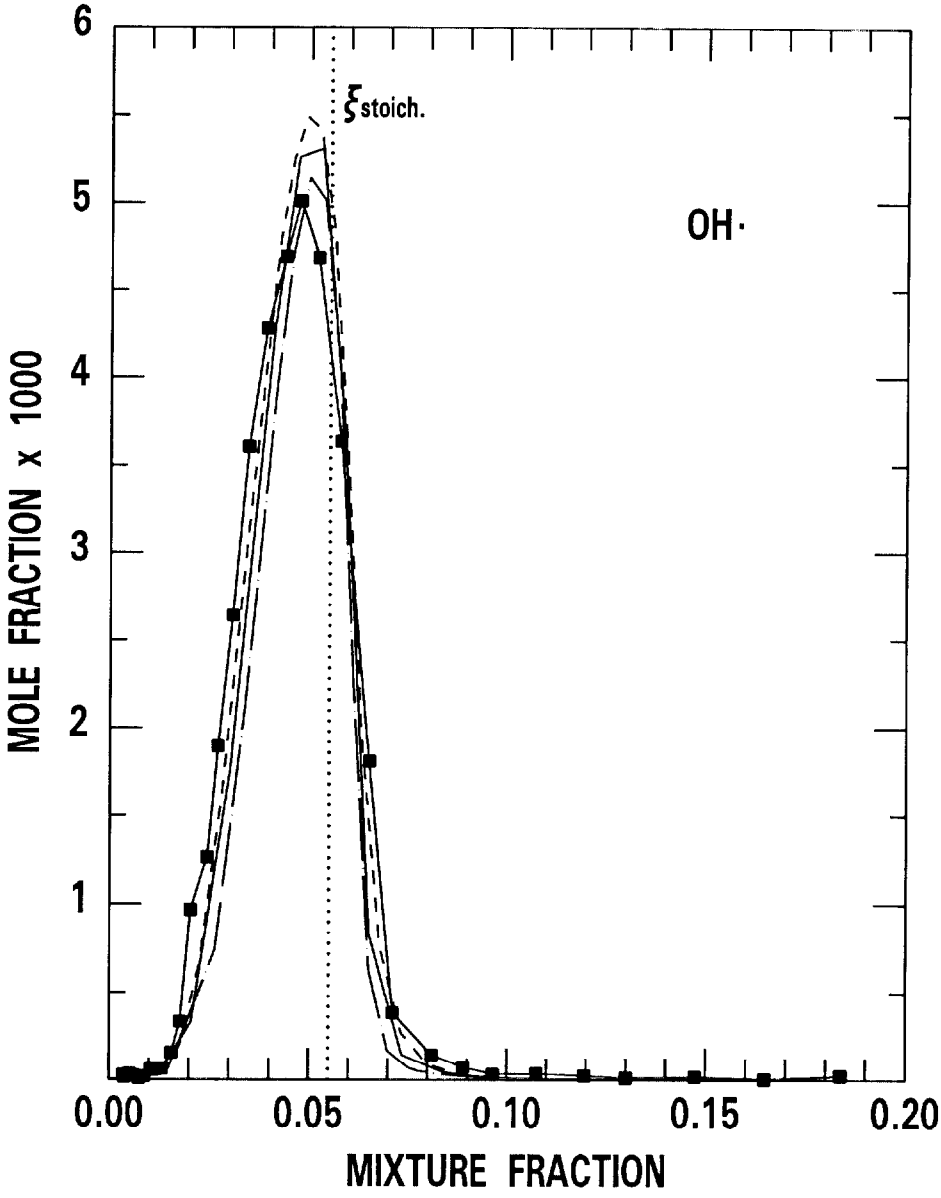

FIGURE 9 Quantitative OH· measurements (Smyth *et al.*, 1990, ■) versus flame structure calculations. The computations are presented for three values of the scalar dissipation rate at the stoichiometric surface: $\chi_s = 0.26\ s^{-1}$ (dash-dot line), $\chi_s = 0.63\ s^{-1}$ (solid line), and $\chi_s = 1.5\ s^{-1}$ (dashed line). The vertical dotted line denotes the location of the stoichiometric mixture fraction, $\xi_s = 0.055$.

in rich flame regions even for the minimum usable intensity of 1.7×10^8 W/cm^2. Various experiments ruled out the photolytic production of O atoms from O_2, NO, and H_2O at a wavelength of 226 nm for our experimental conditions. Other possible photolytic precursors are CH_2O and CO (the latter is unlikely due to poor Franck-Condon overlap;

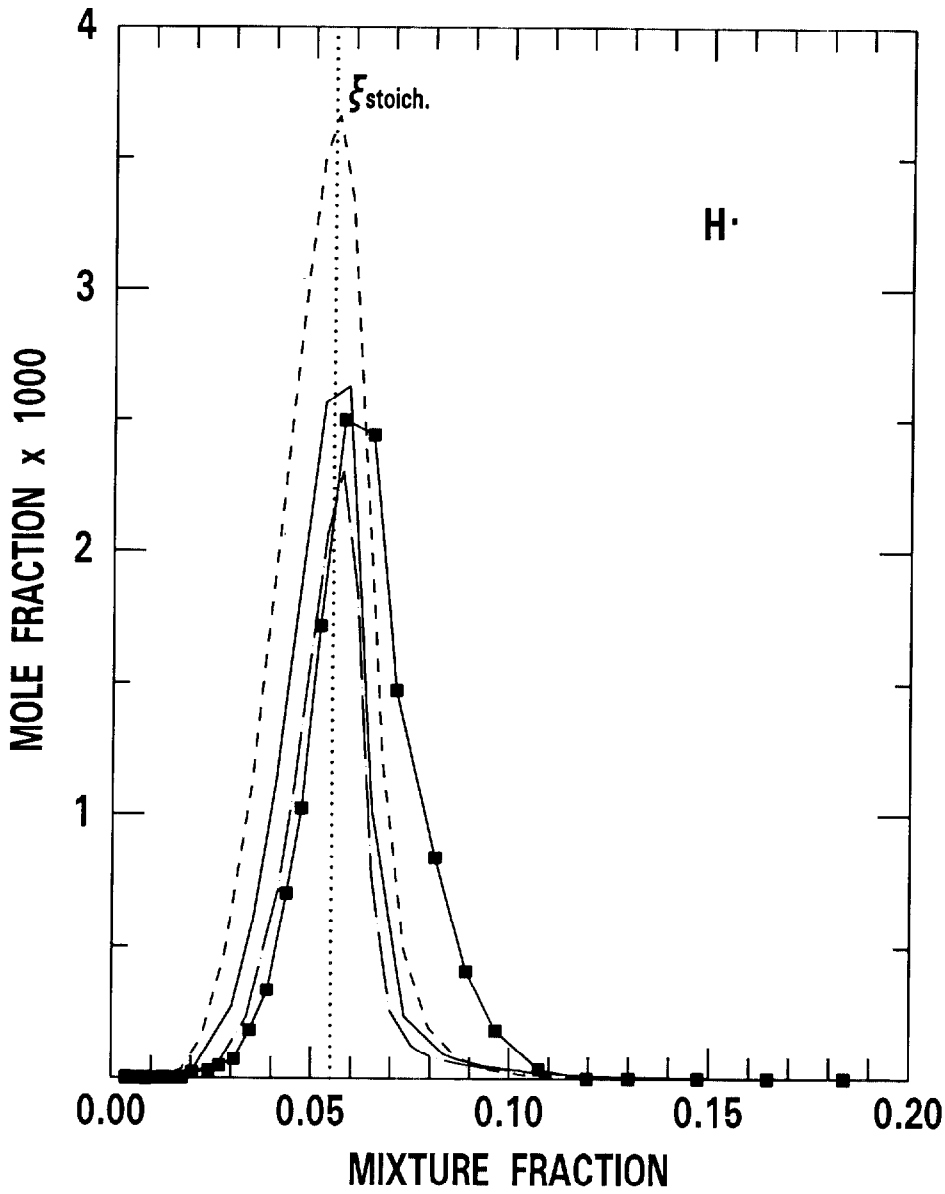

FIGURE 10 Relative H-atom experimental measurements (Smyth and Tjossem, 1990a) scaled to the predicted R3 maximum concentration of 2.5×10^{-3} mole fraction (■ ; see text) versus flame structure calculations. The computations are presented for three values of the scalar dissipation rate at the stoichiometric surface: $\chi_s = 0.26\ s^{-1}$ (dash-dot line), $\chi_s = 0.63\ s^{-1}$ (solid line), and $\chi_s = 1.5\ s^{-1}$ (dashed line). The vertical dotted line denotes the location of the stoichiometric mixture fraction, $\xi_s = 0.055$.

Tjossem and Smyth, 1989). The tail which extends into the rich flame region of the experimental O-atom profile is thus suspect and also is the only significant point of disagreement with the calculated profiles. In Fig. 11 the peak O-atom concentration

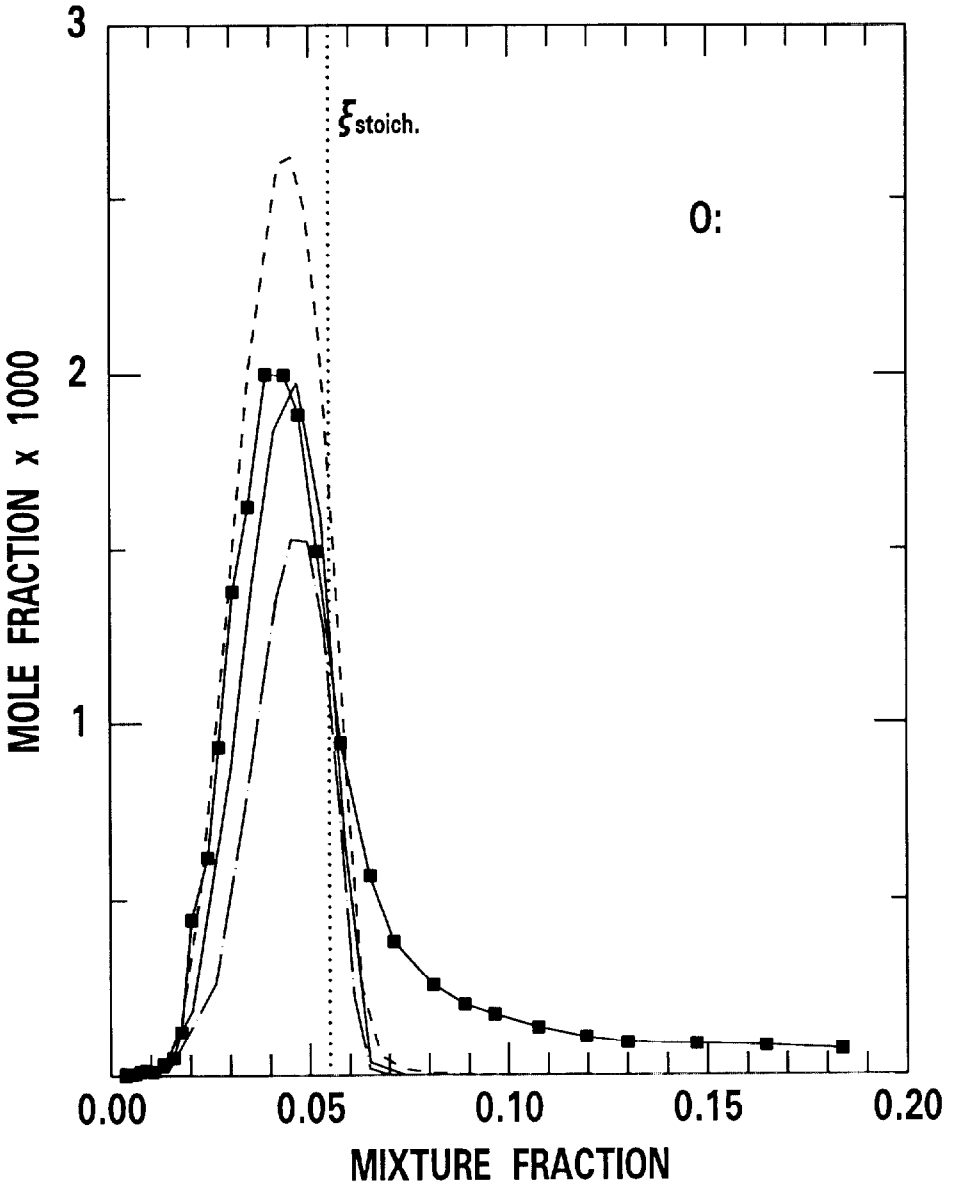

FIGURE 11 Relative O-atom experimental measurements (Smyth and Tjossem, 1990a, ■) scaled to a peak mole fraction of 2.0×10^{-3} (see text) versus flame structure calculations. The computations are presented for three values of the scalar dissipation rate at the stoichiometric surface: $\chi_s = 0.26\ s^{-1}$ (dash-dot line), $\chi_s = 0.63\ s^{-1}$ (solid line), and $\chi_s = 1.5\ s^{-1}$ (dashed line). The vertical dotted line denotes the location of the stoichiometric mixture fraction, $\xi_s = 0.055$.

has been scaled arbitrarily to a mole fraction of 2×10^{-3}, which is between two partial equilibrium estimates which can be made from our flame data (0.80 and 5.3×10^{-3}; Smyth *et al.*, 1990). The location and shape of the experimental and calculated O-atom

profiles are in excellent agreement for mixture fraction values as large as $\xi = 0.06$.

The calculated peak concentrations of both H atom and O atom are more sensitive to the local scalar dissipation rate than is that of OH·. However, experimental profiles have not been obtained over a wide range of heights above the burner for comparison.

2. CH· and CH_3.

Our laser-induced fluorescence data on CH· give the narrowest spatial profile for any species measured in this CH_4/air diffusion flame (Norton and Smyth, 1991). Nevertheless, Fig. 12 shows that the experimental result is considerably broader than the calculated profile in terms of the mixture fraction. The difference cannot be explained as arising from the finite laser beam diameter of approximately 0.1 mm (Norton and Smyth, 1991), which corresponds to a mixture fraction width of only 4×10^{-3} at the location of the maximum CH· concentration. In addition, the computed peak concentrations are at least twice as high as the experimental estimate and occur at leaner flame locations. The maximum CH· concentration is found to be quite sensitive to the local scalar dissipation rate in both the experimental data and the computations, decreasing rapidly with increasing height above the burner as the strain rate decreases.

No quantitative measurements have been reported for the CH· radical in diffusion flames. Our analysis of the chemical reactions which produce and destroy CH· gives a range of values for the ratio $[^3CH_2{:}]_{max}/[CH\cdot]_{max}$ between 13 and 300, depending upon which rate constant recommendations are used (Norton and Smyth, 1991). For the specific values employed in the flame structure computation this ratio is 65. If $[^3CH_2{:}]_{max}$ is taken to be the calculated value of 17.2 ppm for the best matched axial location, then our experimental estimate of $[CH\cdot]_{max}$ becomes 0.26 ppm at a height of 9 mm above the burner. In Fig. 12 the relative experimental profile has been scaled to this result. The computed maximum CH· concentration is 0.52 ppm at the flame location with best matched overall scalar dissipation rate; a finer computational grid would likely increase this value to approximately 0.7 ppm. This agreement is quite good considering the high sensitivity of the CH· concentration to the local strain rate and the wide range of reported rate constants for CH· reactions (Norton and Smyth, 1991).

Figure 13 compares our experimental data on the methyl radical from both the multiphoton ionization (Smyth and Norton, 1990) and the quartz microprobe scavenger sampling experiments (Miller and Taylor, 1987) with the calculated profiles. The optical and mass spectrometric measurements agree well with each other in terms of their location and their profile shapes. These experimental data have been scaled to the same peak value, which is 20 times higher than a lower bound estimate of 1.1×10^{-4} derived from the CH_3I concentration measured in an I_2 scavenging experiment (Miller and Taylor, 1987). A second mass spectrometric estimate of the maximum CH_3· mole fraction of 5.5×10^{-4} at H = 9 mm has been made from methyl radical recombination to produce C_2H_6 (Smyth and Taylor, 1985). These values should be reduced by 14% due to the mole sum correction applied to all of our mass spectrometric data, discussed in Section II.D. In contrast, the flame structure calculation gives a much larger value for the maximum CH_3· mole fraction of 2.3×10^{-3} at the best matched axial location. Although the experimental measurements are strictly lower bounds, the wide discrepancy of at least a factor of four (for the larger mass spectrometric estimate) is surprising.

The experimental location of the peak methyl radical concentration occurs at a slightly richer mixture fraction than the calculated maximum, while the shapes of the experimental and computed profiles agree closely. For the computed profiles the shape and peak concentrations are quite sensitive to the scalar dissipation rate. However, the multiphoton ionization data and the mass spectrometric measurements do not show decreasing methyl radical concentrations with increasing height in the flame (i.e.,

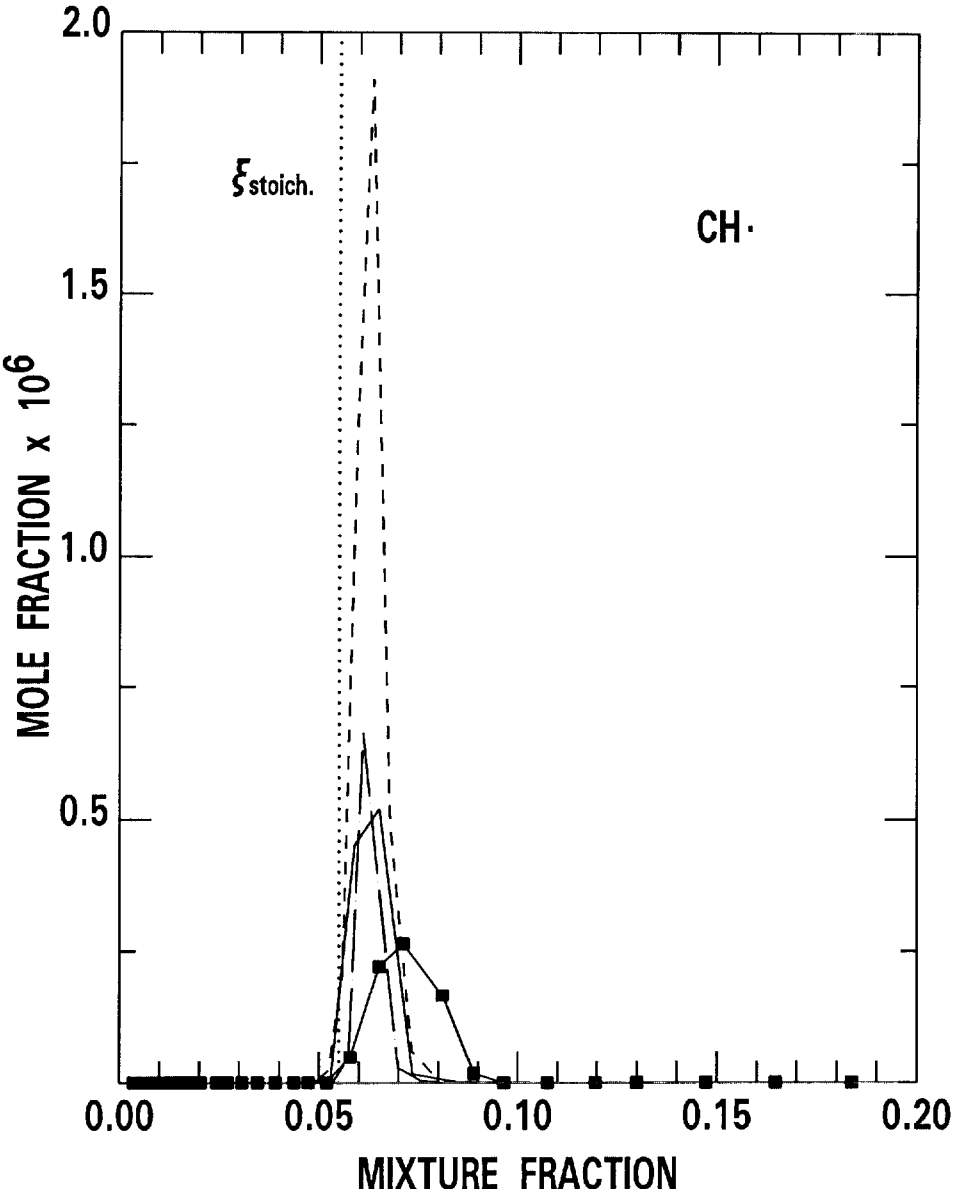

FIGURE 12 Relative CH· experimental measurements (Norton and Smyth, 1991) scaled to a peak mole fraction of 2.6×10^{-7} mole fraction (■ ; see text) versus flame structure calculations. The computations are presented for three values of the scalar dissipation rate at the stoichiometric surface: $\chi_s = 0.26\ s^{-1}$ (dash-dot line), $\chi_s = 0.63\ s^{-1}$ (solid line), and $\chi_s = 1.5\ s^{-1}$ (dashed line). The vertical dotted line denotes the location of the stoichiometric mixture fraction, $\xi_s = 0.055$.

decreasing scalar dissipation rate). Clearly, an absolute experimental measurement of the CH_3· concentration, for example using tunable diode laser spectroscopy, is desirable.

The comparison between the experimental and calculated profiles for the CH· and CH_3·

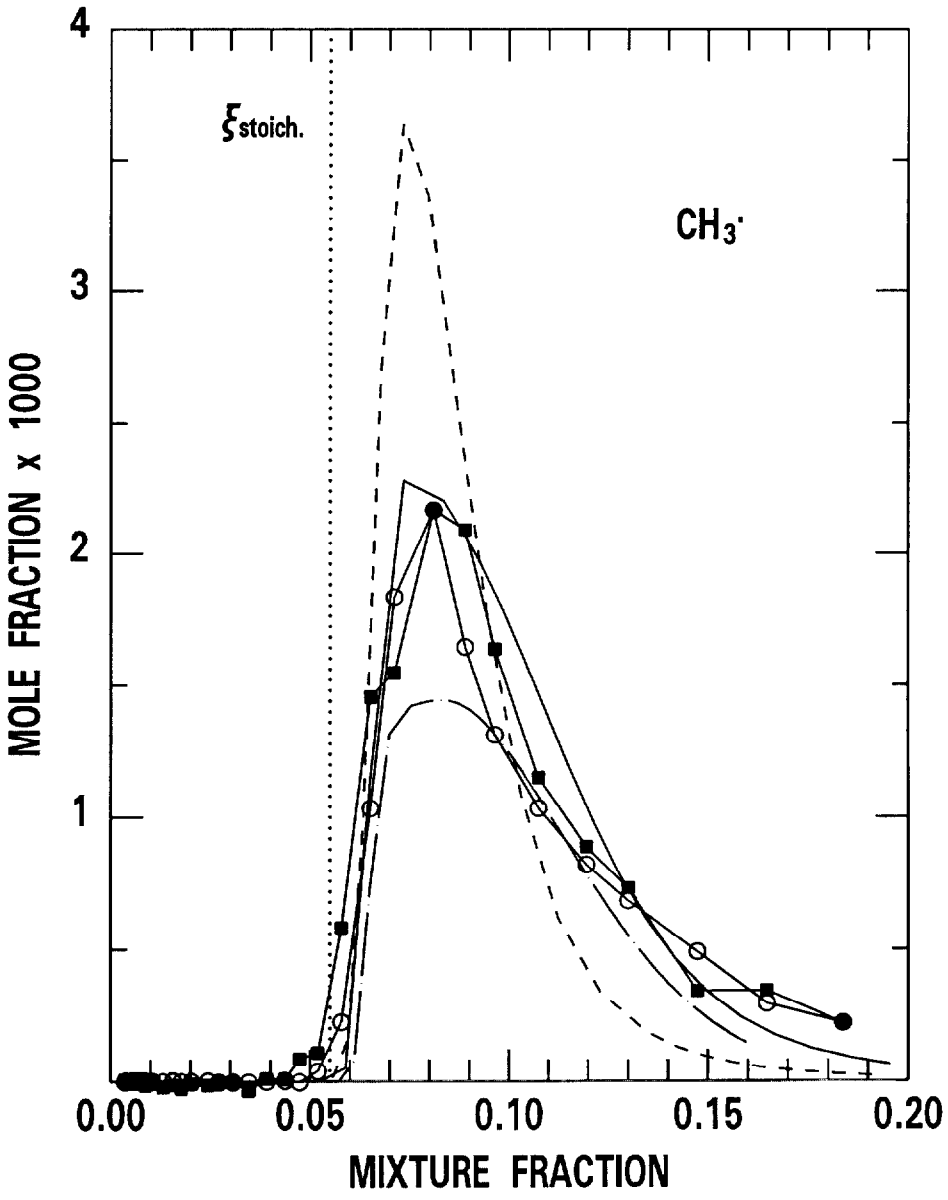

FIGURE 13 Quantitative mass spectrometric lower limit CH_3· measurements (Miller and Taylor, 1987, ■) multiplied by a factor of 20 and relative multiphoton ionization data (Smyth and Norton, 1990) scaled to the same peak concentration (o) versus flame structure calculations. The computations are presented for three values of the scalar dissipation rate at the stoichiometric surface: $\chi_s = 0.26\ s^{-1}$ (dash-dot line), $\chi_s = 0.63\ s^{-1}$ (solid line), and $\chi_s = 1.5\ s^{-1}$ (dashed line). The vertical dotted line denotes the location of the stoichiometric mixture fraction, $\xi_s = 0.055$.

radicals is less satisfactory than is the case for OH·, H atom, and O atom. The computed concentrations of these radicals are particularly sensitive to the local strain rate. Possible

reasons for the disagreement include the limited number of chemical reactions used in the flame structure calculation, as well as geometric differences between the experimental and computed flame structures which are not accounted for by matching regions of scalar dissipation rate. It has proven to be difficult to estimate absolute CH· concentrations in CH_4/air diffusion flames. For example, accurate steady-state expressions have not been successfully derived from reduced chemical mechanisms (Norton and Smyth, 1991).

VI CONCLUSIONS

Experimental measurements are compared to computed species concentration profiles for different two-dimensional CH_4/air diffusion flames burning at atmospheric pressure. The experimental data were obtained using a rectangular Wolfhard-Parker burner with a flame height of approximately 33 cm, while the computation has been carried out for a 3.8 cm tall axisymmetric flame. Comparisons of temperature and species concentrations can be made by basing the analysis on the local flame conditions, specifically the mixture fraction and the scalar dissipation rate. The best method for establishing a basis of comparison for the scalar dissipation rate involves using a least-squares procedure over a range of mixture fraction, rather than matching at a specific point which corresponds to the stoichiometric surface or the temperature maximum.

Good agreement is found for the major radical species OH·, H atom, and O atom, while for the hydrocarbon radicals CH· and CH_3· some features of the profiles agree well but significant areas of disagreement exist. Overall, the calculated positions of the peak radical concentrations are slightly more compressed in terms of the mixture fraction compared to the experimental results. The predicted concentration profiles for the major species certainly agree with the experimental measurements as well as found in investigations on premixed flames, for example in acetylene combustion (Westmoreland *et al.*, 1986). The model results are somewhat more sensitive to the scalar dissipation rate than are the experimental profiles.

The most serious areas of disagreement concern the comparison of the temperature profiles and the much larger degree of O_2 penetration in the computed flame structure. The influence of the latter, particularly in rich flame regions, is likely to be small and can be further investigated by carrying out one-dimensional counterflow calculations with and without a small amount of O_2 added to the fuel stream and then comparing species profiles. Given the importance of the temperature field in determining the chemical structure of a diffusion flame, the disagreement between the computed and the experimental temperature profiles certainly deserves further study before one can be satisfied with the generally excellent agreement for the individual species profiles.

REFERENCES

Barlow, R. S., Dibble, R. W., Stårner, S. H., and Bilger, R. W. (1990a). Piloted Diffusion Flames of Nitrogen-Diluted Methane Near Extinction: OH Measurements. *Twenty-Third Symposium (International) on Combustion*, The Combustion Institute, Pittsburgh, PA, p. 583.

Barlow, R. S., Dibble, R. W., Stårner, S. H., Bilger, R. W., Fourguette, D. C., and Long, M. B. (1990b). Reaction Zone Structure in Dilute Methane Jet Flames Near Extinction. AIAA Paper 90-0732.

Barlow, R. S. and Collignon, A. (1991). Linear LIF Measurements of OH in Nonpremixed Methane-Air Flames: When Are Quenching Corrections Unnecessary? AIAA Paper 91-0179.

Barlow, R. S., Stårner, S. H., and Bilger, R. W. (1991). An Experimental Study of Laminar, Transitional, and Turbulent Jet Flames of Air-Diluted Methane. Spring meeting of the Western States section of the Combustion Institute, paper #91-14.

Bastin, E., Delfau, J.-L., Reuillon, M., and Vovelle, C. (1987). Mass Spectrometric Analysis of the Structure of a $C_2H_2/O_2/Ar$ Diffusion Flame. *Journal de Chimie Physique* **84**, 415.

Bilger, R. W. (1976). The Structure of Diffusion Flames. *Combustion Science and Technology* **13**, 155.

Bilger, R. W. (1977). Reaction Rates in Diffusion Flames. *Combustion and Flame* **30**, 277.

Bilger, R. W. (1988). The Structure of Turbulent Nonpremixed Flames. *Twenty-Second Symposium (International) on Combustion,* The Combustion Institute, Pittsburgh, PA, p. 475.

Bilger, R. W., Stårner, S. H., and Kee, R. J. (1990). On Reduced Mechanisms for Methane-Air Combustion in Nonpremixed Flames. *Combustion and Flame* **80,** 135.

Biordi, J. C., Lazzara, C. P., and Papp, J. F. (1977). An Examination of the Partial Equilibration Hypothesis and Radical Recombination in 1/20 atm Methane Flames. *Sixteenth Symposium (International) on Combustion,* The Combustion Institute, Pittsburgh, PA, p. 1097.

Bittner, J. D. (1981). A Molecular Beam Mass Spectrometer Study of Fuel-Rich and Sooting Benzene-Oxygen Flames. D.Sc. Dissertation, Massachusetts Institute of Technology.

Calcote, H. F., Olson, D. B., and Keil, D. G. (1988). Are Ions Important in Soot Formation? *Energy and Fuels* **2,** 494.

Delfau, J.-L. and Vovelle, C. (1984). Mechanism of Soot Formation in Premixed C_2H_2/O_2 Flames. *Combustion Science and Technology* **41,** 1.

Drake, M. C. (1986). Stretched Laminar Flamelet Analysis of Turbulent H_2 and $CO/H_2/N_2$ Diffusion Flames. *Twenty-First Symposium (International) on Combustion,* The Combustion Institute, Pittsburgh, PA, p. 1579.

Drake, M. C. and Blint, R. J. (1991). Relative Importance of Nitric Oxide Formation Mechanisms in Laminar Opposed-flow Diffusion Flames. *Combustion and Flame* **83,** 185.

Dreier, T., Lange, B., Wolfrum, J., Zahn, M., Behrendt, F., and Warnatz, J. (1986). CARS Measurements and Computations of the Structure of Laminar Stagnation-Point Methane-Air Counterflow Diffusion Flames. *Twenty-First Symposium (International) on Combustion,* The Combustion Institute, Pittsburgh, PA, p. 1729.

Faris, G. W. and Byer, R. L. (1987). Beam-Deflection Optical Tomography of a Flame. *Optics Letters* **12,** 155.

Farrow, R. L., Mattern, P. L., and Rahn, L. A. (1982). Comparison between CARS and Corrected Thermocouple Temperature Measurements in a Diffusion Flame. *Applied Optics* **21,** 3119.

Fristrom, R. M. and Westenberg, A. A. (1965). *Flame Structure,* McGraw-Hill, New York, chapter 5.

Hamins, A., Anderson, D. T., and Miller, J. H. (1990). Mechanistic Studies of Toluene Destruction in Diffusion Flames. *Combustion Science and Technology* **71,** 175.

Haworth, D. C., Drake, M. C., and Blint, R. J. (1988). Stretched Laminar Flamelet Modeling of a Turbulent Jet Diffusion Flame. *Combustion Science and Technology* **60,** 287.

Hirschfelder, J. O., Curtiss, C. F., and Bird, R. B. (1954). *Molecular Theory of Gases and Liquids.* John Wiley and Sons, Inc., New York.

Kee, R. J., Warnatz, J., and Miller, J. A. (1983). A FORTRAN Computer Code Package for the Evaluation of Gas-Phase Viscosities, Conductivities, and Diffusion Coefficients. Sandia National Laboratories Report SAND83-8209.

Kent, J. H., Jander, H., and Wagner, H. Gg. (1981). Soot Formation in a Laminar Diffusion Flame. *Eighteenth Symposium (International) on Combustion,* The Combustion Institute, Pittsburgh, PA, p. 1117.

Lawitzki, A., Plath, I., Strickler, W., Bittner, J., Meier, U., and Kohse-Höinghaus, K. (1990). Laser-Induced Fluorescence Determination of Flame Temperatures in Comparison with CARS Measurements. *Applied Physics B* **50,** 513.

Liew, S. K., Bray, K. N. C., and Moss, J. B. (1981). A Flamelet Model of Turbulent Non-Premixed Combustion. *Combustion Science and Technology* **27,** 69.

Liew, S. K., Bray, K. N. C., and Moss, J. B. (1984). A Stretched Laminar Flamelet Model of Turbulent Nonpremixed Combustion. *Combustion and Flame* **56,** 199.

Madson, J. M. and Theby, E. A. (1984). SiO_2 Coated Thermocouples. *Combustion Science and Technology* **36,** 205.

Melvin, A. and Moss, J. B. (1975). Structure in Methane-Oxygen Diffusion Flames. *Fifteenth (International) Symposium on Combustion,* The Combustion Institute, Pittsburgh, PA, p. 625.

Miller, J. A. and Bowman, C. T. (1989). Mechanism and Modelling of Nitrogen Chemistry in Combustion. *Progress in Energy and Combustion Science* **15,** 287.

Miller, J. H., Elreedy, S., Ahvazi, B., Woldu, F., and Hassanzadeh, P. (1992). Tunable Diode Laser Measurement of Carbon Monoxide Concentration and Temperature in a Laminar Methane/Air Diffusion Flame, *Applied Optics,* in press.

Miller, J. H., Mallard, W. G., and Smyth, K. C. (1986). Chemical Production Rates of Intermediate Hydrocarbons in a Methane/Air Diffusion Flame. *Twenty-First Symposium (International) on Combustion,* The Combustion Institute, Pittsburgh, PA, p. 1057.

Miller, J. H. and Smyth, K. C. (1990). Comparisons of Methane/Air Flame Diffusion Structure Data with Predictions of "Full" Chemical Mechanisms. Eastern States Combustion Institute Meeting, Orlando, FL, Paper #37.

Miller, J. H. and Taylor, P. H. (1987). Methyl Radical Concentrations and Production Rates in a Laminar Methane/Air Diffusion Flame. *Combustion Science and Technology* **52,** 139.

Mitchell, R. (1979). Theoretical Model of Chemically Reacting, Recirculating Flows. Sandia National Laboratories Report SAND79-8236.

Mitchell, R. E., Sarofim, A. F., and Clomburg, L. A. (1980). Experimental and Numerical Investigation of Confined Laminar Diffusion Flames. *Combustion and Flame* **37,** 227.

Norton, T. S. and Smyth, K. C. (1991). Laser-Induced Fluorescence of CH· in a Laminar CH_4/Air Diffusion Flame: Implications for Diagnostic Measurements and Analysis of Chemical Rates. *Combustion Science and Technology* **76,** 1.

Paczko, G., Lefdal, P. M., and Peters, N. (1986). Reduced Reaction Schemes for Methane, Methanol, and Propane Flames. *Twenty-First Symposium (International) on Combustion,* The Combustion Institute, Pittsburgh, PA, p. 739.

Peters, N. (1984). Laminar Diffusion Flamelet Models in Non-Premixed Turbulent Combustion. *Progress in Energy and Combustion Science* **10,** 319.

Peters, N. (1986). Laminar Flamelet Concepts in Turbulent Combustion. *Twenty-First Symposium (International) on Combustion,* The Combustion Institute, Pittsburgh, PA, p. 1231.

Peters, N. and Kee, R. J. (1987). The Computation of Stretched Laminar Methane-Air Diffusion Flames Using a Reduced Four-Step Mechanism. *Combustion and Flame* **68,** 17.

Peters, N. (1990). Personal communication.

Puri, I. K., Seshadri, K., Smooke, M. D., and Keyes, D. E. (1987). A Comparison Between Numerical Calculations and Experimental Measurements of the Structure of a Counterflow Methane-Air Diffusion Flame. *Combustion Science and Technology* **56,** 1.

Rogg, B., Behrendt, F., and Warnatz, J. (1986). Turbulent Non-Premixed Combustion in Partially Premixed Diffusion Flamelets with Detailed Chemistry. *Twenty-First Symposium (International) on Combustion,* The Combustion Institute, Pittsburgh, PA, p. 1533.

Saito, K., Williams, F. A., and Gordon, A. S. (1986). Structure of Laminar Coflow Methane-Air Diffusion Flames. *Journal of Heat Transfer* **108,** 640.

Santoro, R. J. (1991). Personal communication.

Savitzky, A. and Golay, M. J. E. (1964). Smoothing and Differentiation of Data by Simplified Least Squares Procedures. *Analytical Chemistry* **36,** 1627.

Schoenung, S. M. and Hanson, R. K. (1981). CO and Temperature Measurements in a Flat Flame by Laser Absorption Spectroscopy and Probe Techniques. *Combustion Science and Technology,* **24,** 227.

Seshadri, K., Mauβ, F., Peters, N., and Warnatz, J. (1990). A Flamelet Calculation of Benzene Formation in Co-Flowing Laminar Diffusion Flames. *Twenty-Third Symposium (International) on Combustion,* The Combustion Institute, Pittsburgh, PA, p. 559.

Sick, V., Arnold, A., Dieβel, E., Dreier, T., Ketterle, W., Lange, B., Wolfrum, J., Thiele, K. U., Behrendt, F., and Warnatz, J. (1990). Two-Dimensional Laser Diagnostics and Modeling of Counterflow Diffusion Flames. *Twenty-Third Symposium (International) on Combustion,* The Combustion Institute, Pittsburgh, PA, p. 495.

Sivathanu, Y. R. and Faeth, G. M. (1990). Generalized State Relationships for Scalar Properties in Nonpremixed Hydrocarbon/Air Flames. *Combustion and Flame* **82,** 211.

Smooke, M. D., editor (1991). *Reduced Kinetic Mechanisms and Asymptotic Approximations for Methane-Air Flames,* Lecture Notes in Physics Vol. 384, Springer-Verlag Berlin.

Smooke, M. D., Mitchell, R. E., and Keyes, D. E. (1989). Numerical Solution of Two-Dimensional Axisymmetric Laminar Diffusion Flames. *Combustion Science and Technology* **67,** 85.

Smooke, M. D., Lin., P., Lam, J. K., and Long, M. B. (1990). Computational and Experimental Study of a Laminar Axisymmetric Methane-Air Diffusion Flame. *Twenty-Third Symposium (International) on Combustion,* The Combustion Institute, Pittsburgh, PA, p. 575.

Smyth, K. C., Miller, J. H., Dorfman, R. C., Mallard, W. G., and Santoro, R. J. (1985). Soot Inception in a Methane/Air Diffusion Flame as Characterized by Detailed Species Profiles. *Combustion and Flame* **62,** 157.

Smyth, K. C. and Taylor, P. H. (1985). Detection of the Methyl Radical in a Methane/Air Diffusion Flame by Multiphoton Ionization Spectroscopy. *Chemical Physics Letters* **122,** 518.

Smyth, K. C. and Miller, J. H. (1987). Chemistry of Molecular Growth Processes in Flames. *Science* **236,** 1540.

Smyth, K. C. and Tjossem, P. J. H. (1990a). Relative H-Atom and O-Atom Concentration Measurements in a Laminar, Methane/Air Diffusion Flame. *Twenty-Third Symposium (International) on Combustion,* The Combustion Institute, Pittsburgh, PA, p. 1829.

Smyth, K. C. and Tjossem, P. J. H. (1990b). Signal Detection Efficiency in Multiphoton Ionization Flame Measurements. *Applied Optics* **29,** 4891.

Smyth, K. C., Tjossem, P. J. H., Hamins, A., and Miller, J. H. (1990). Concentration Measurements of OH· and Equilibrium Analysis in a Laminar Methane/Air Diffusion Flame. *Combustion and Flame* **79,** 366.

Smyth, K. C. and Norton, T. S. (1990). Unpublished results.

Syed, K. J., Stewart, C. D., and Moss, J. B. (1990). Modelling Soot Formation and Thermal Radiation in Buoyant Turbulent Diffusion Flames. *Twenty-Third Symposium (International) on Combustion,* The Combustion Institute, Pittsburgh, PA, p. 1533.

Tjossem, P. J. H. and Smyth, K. C. (1989). Multiphoton Excitation Spectroscopy of the $B^1\Sigma^+$ and $C^1\Sigma^+$ Rydberg States of CO. *Journal of Chemical Physics* **91**, 2041.

Wang, H. and Frenklach, M. (1991). Detailed Reduction of Reaction Mechanisms for Flame Modeling. *Combustion and Flame* **87**, 365.

Westmoreland, P. R., Howard, J. B., and Longwell, J. P. (1986). Tests of Published Mechanisms by Comparison with Measured Laminar Flame Structure in Fuel-Rich Acetylene Combustion. *Twenty-First Symposium (International) on Combustion*, The Combustion Institute, Pittsburgh, PA, p. 773.

Williams, F. A. (1985). *Combustion Theory*. 2nd edition, Benjamin/Cummings, Menlo Park, CA.